JOURNAL OF GEOPHYSICAL RESEARCH, VOL. 106, NO. D12, PAGES 12,643-12,660, JUNE 27, 2001

Global tropospheric NO_2 column distributions: Comparing three-dimensional model calculations with GOME measurements

Guus J. M. Velders,[1,2] Claire Granier,[2,3,4] Robert W. Portmann,[2] Klaus Pfeilsticker,[2,5] Mark Wenig,[5] Thomas Wagner,[5] Ulrich Platt,[5] Andreas Richter,[6] and John P. Burrows[6]

Abstract. Tropospheric NO_2 columns derived from the data products of the Global Ozone Monitoring Experiment (GOME), deployed on the ESA ERS-2 satellite, have been compared with model calculations from two global three-dimensional chemistry transport models, IMAGES and MOZART. The main objectives of the study are an analysis of the tropospheric NO_2 data derived from satellite measurements, an interpretation of it and evaluation of its quality using global models, and an estimation the role of NO_2 in radiative forcing. The measured and modeled NO_2 columns show similar spatial and seasonal patterns, with large tropospheric column amounts over industrialized areas and small column amounts over remote areas. The comparison of the absolute values of the measured and modeled tropospheric column amounts are particularly dependent upon uncertainties in the derivation of the tropospheric NO_2 columns from GOME and the difficulty of modeling the boundary layer in global models, both of which are discussed below. The measured tropospheric column amounts derived from GOME data are of the same order as those calculated by the MOZART model over the industrialized areas of the United States and Europe, but a factor of 2-3 larger for Asia. The modeled tropospheric NO_2 columns from MOZART as well as the column amounts measured by GOME are in good agreement with NO_2 columns derived from observed NO_2 mixing ratios in the boundary layer in eastern North America. The comparison of the models to the GOME data illustrates the degree to which present models reproduce the hot spots seen in the GOME data. The radiative forcing of NO_2 has been estimated from the calculated tropospheric NO_2 columns. The local maxima in the radiative forcing of tropospheric NO_2 for cloud-free conditions over the eastern United States and western Europe represent 0.1-0.15 W m^{-2}, while values of 0.04-0.1 W m^{-2} are estimated on a continental scale in these regions, of the same order of magnitude as the forcing of N_2O and somewhat smaller than the regional forcing of tropospheric ozone. The globally averaged radiative forcing of tropospheric NO_2 is negligible, ~0.005 W m^{-2}.

1. Introduction

Nitrogen dioxide (NO_2) plays a key role in tropospheric chemistry. For example, its photolysis leads to the formation of ozone (O_3) and its reaction with the hydroxyl radical (OH) produces nitric acid (HNO_3). These processes are of importance in both the planetary boundary layer and free troposphere [e.g., *Chameides et al*., 1992]. Thereby NO_2 participates in the control of the strong oxidant, O_3, and the strongest atmospheric oxidizing agent, OH, and plays an important part in determining the oxidizing capacity of the atmosphere [*Logan et al*., 1981]. Recently, it has been recognized that NO_2 contributes both directly and indirectly to the radiative forcing of climate [*Solomon et al*., 1999]. In addition, it is known that in high concentration, NO_2 causes respiratory problems for humans [e.g., *Environmental Protection Agency (EPA)*, 1998].

As both the atmospheric sources and sinks of NO_2 are strongly non homogeneously distributed, the concentration of NO_2 in the troposphere is highly variable, both spatially and temporally [e.g., *Emmons et al*., 1997]. In the boundary layer above industrialized areas, values up to several tens of ppbv are observed having a strong diurnal variation, whereas in remote areas the concentrations are typically in the range of 10-200 pptv. Prior to the advent of space-based remote sensing instrumentation such as the Global Ozone Monitoring Experiment (GOME), and because of its high intrinsic variability and consequent sparse set of in situ or remote sensing measurements, global knowledge about the amount

[1]Air Research Laboratory, National Institute of Public Health and the Environment (RIVM), Bilthoven, Netherlands.
[2]Aeronomy Laboratory, NOAA, Boulder, Colorado.
[3]Service d'Aéronomie, Centre National de la Recherche Scientifique, Paris, France.
[4]Cooperative Institute for Research in Environmental Science, University of Colorado, Boulder, Colorado.
[5]Institut für Umweltphysik, University of Heidelberg, Heidelberg, Germany.
[6]Institute of Environmental Physics, University of Bremen, Bremen, Germany.

Paper number 2000JD900762.
0148-0227/01/2000JD900762$09.00

and distribution of NO_2 has been difficult if not impossible to obtain. In several recent studies [*Horowitz and Jacob*, 1999; *Levy et al*., 1999; *Penner et al*., 1998; *Wang et al*., 1998; *Kraus et al*., 1996; *Lamarque et al*., 1996], chemistry transport models have been used to calculate the global three-dimensional distribution of tropospheric NO_x and study its sources, sinks, and atmospheric transport.

GOME [*Burrows et al.,* 1991, 1993, 1999] is a small scale version of the Scanning Imaging Absorption Spectrometer for Atmospheric Chartography (SCIAMACHY) [*Bovesmann et al*., 1999] observing between 232 and 793 nm and only in nadir viewing geometry. It measures the radiance upwelling from the atmosphere and the extraterrestrial solar irradiance. Appropriate inversion of these data products yields global information about the atmospheric absorption and scattering processes enabling the abundance of trace constituents such as O_3 and NO_2 to be retrieved.

The GOME measurements have been used in this study to determine the NO_2 tropospheric column distribution on a global scale. The retrieval of these unique data is just now possible with the measurements of the GOME instrument. In addition, two three-dimensional global chemistry transport models IMAGES (Intermediate Model for the Global Evolution of Species) [*Müller and Brasseur*, 1995; *Pham et al*., 1995; *Granier et al*., 1996, 1999, 2000a, 2000b] and MOZART (Model for Ozone and Related Chemical Tracers) [*Brasseur et al*., 1998; *Hauglustaine et al*., 1998] have been used to investigate the retrieved tropospheric NO_2 column amounts and help to interpret it. Both models use the EDGAR emission database [*Olivier et al*., 1996] for anthropogenic emissions and the database developed by *Müller* [1992] for natural emissions. The main differences between these models are the source of the atmospheric wind fields (monthly mean climatological fields for IMAGES and 6 hourly fields from a global circulation model for MOZART) and the representation of the boundary layer. MOZART has a less diffusive boundary layer than IMAGES, resulting in a more realistic representation of the physical and chemical processes in the lowest layers of the model.

In this decade a number of satellite instruments will be launched into low Earth orbit whose primary objective is to investigate the trace gas distributions in the lower troposphere, e.g., SCIAMACHY on ENVISAT [*Bovesmann et al*., 1999, and references therein], GOME-2 on METOP, Ozone Monitoring Instrument (OMI), and Tropospheric Emission Spectrometer (TES) on EOS-CHEM. An adequate understanding of atmospheric radiative transfer, in particular, in the boundary layer, is required to interpret accurately the slant column amounts from these nadir sounding instruments.

In this study the global distribution of tropospheric NO_2 column amounts retrieved from GOME level 1 data products have been compared with NO_2 column amounts inferred from three-dimensional chemistry transport models. Investigating the similarities and differences in the magnitude, global distribution, and seasonal variations of the retrieved and simulated NO_2 provides novel insight into the global behavior of NO_x. Importantly, the GOME tropospheric NO_2 columns reveal "hotspots" of significance for the assessment of regional, transnational, and intercontinental air pollution.

The algorithms used to retrieve NO_2 column amounts from GOME observations are discussed in section 2. Section 3 describes the chemistry transport models IMAGES and MOZART. In section 4 modeled (IMAGES and MOZART) and observed (GOME) NO_2 column amounts are compared. The contributions of the different atmospheric model layers to the total tropospheric NO_2 column amounts and the different factors affecting the simulated NO_2 columns are discussed in section 5, followed by a comparison of the modeled NO_2 data with observations in section 6. The effect of the NO_2 columns on the radiative forcing of climate is probed in section 7, and section 8 summarizes the major conclusions to be drawn from our study.

2. Tropospheric NO_2 Columns Retrieved From GOME

In this section, the GOME instrument and its measurements are described, the retrieval methods applied to the GOME observations are discussed, and the resultant monthly averaged tropospheric NO_2 vertical column densities (VCDs) for 1997 are presented. As a large part of the tropospheric NO_2 column over polluted areas is believed to be located in the boundary layer, the sensitivity of GOME data to uncertainties in the retrieval of NO_2 in the boundary layer is considered and an estimate of the total tropospheric NO_2 VCD made, which accounts for clouds covering its source regions during the GOME overpasses.

Tropospheric NO_2 plumes typically occur on regional and continental scales, as shown in Plates 1c and 2 where locally large amounts are observed over Europe, eastern North America, parts of Asia, and the Johannesburg metropolitan area in South Africa. More than 90% of the tropospheric NO_2 is believed to be emitted into continental air, while the remaining 10% is generated over the ocean by lightning, and ship or aircraft emissions [e.g., *Valks and Velders*, 1999]. In contrast, stratospheric NO_x results largely from the reaction of nitrous oxide (N_2O) with excited oxygen atoms. In addition, the relatively short lifetime of NO_x in the troposphere, compared to that in the stratosphere, leads to its tropospheric distribution appearing as plumes emanating from source regions.

Over populated regions of the continents the majority of the NO_2 column is released from and believed to be located primarily in the boundary layer, with smaller amounts being transported to or generated in the free troposphere and stratosphere. In the remote maritime atmosphere the only significant source of tropospheric NO_2 is in-cloud lightning and transport from the continents. Analysis of both models of the stratospheric NO_2 behavior and the UARS HALOE NO_2 data products reveals that the NO_2 column in the upper atmosphere has significant longitudinal homogeneity up to and beyond latitudes of 65° for the same solar zenith angle. This is explained by the fact that the majority of this NO_2 is located in the middle and upper stratosphere, where it is relatively unperturbed by local changes in the troposphere, but strongly influenced by the solar zenith angle. In addition, advective mixing of NO_x at such altitudes is relatively rapid compared to the rate of its chemical production or loss.

The assumptions that the upper atmospheric column of NO_2 is longitudinally homogeneous and that tropospheric amounts of NO_2 above the clean remote ocean are small provide the physical basis enabling the tropospheric and stratospheric NO_2 columns to be separated from the inversion of nadir observations of GOME or SCIAMACHY. Two related but independent approaches have been used in this study. They both utilize the GOME level 1 data products: the

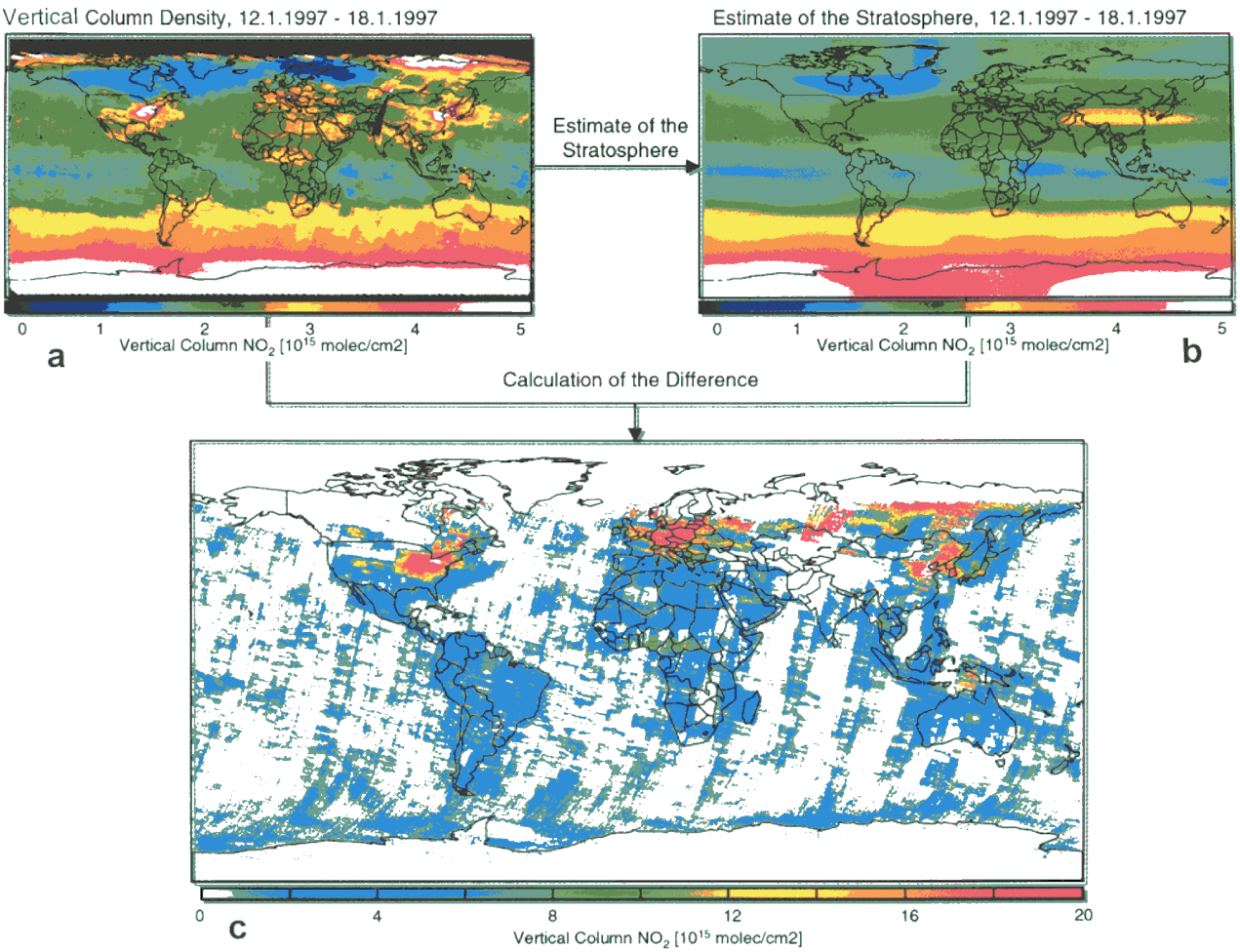

Plate 1. Flowchart of the steps in the algorithm to separate the stratospheric and tropospheric parts of the GOME NO_2 column. (a) the land masses and cloudy pixels are masked out and (b) the stratosphere is estimated using a normalized convolution. (c) The tropospheric residual is then estimated by calculating the difference between Plates 1a and 1b. Plate 1c shows the GOME tropospheric NO_2 column with the correct air mass factors depending on solar zenith angle, ground albedo and clouds. Note the different scales of the maps.

top of the atmosphere radiance (TOARAD), observed from the GOME viewing geometry, and the extra-terrestrial solar irradiance (ETSIR).

2.1. GOME Instrument and Observations

The GOME instrument, on board the second European Research Satellite (ERS-2) comprises a scanning mirror, spectrometer, thermal and electronic subsystems [*Burrows et al*., 1991, 1993, 1999]. Light from the atmosphere is collected by the scan mirror then focused on the entrance slit of the spectrometer by an off-axis parabolic telescope. After being collimated, the light passes though a predispersing prism forming an intermediate spectrum within the instrument. The predispersing prism is such that internal reflection results in a polarized beam, which is directed towards the polarization monitoring device (PMD). The latter comprise three broadband detectors, which observe upwelling radiation from the atmosphere polarized relative to plane within the instrument in the wavelength ranges 300-400 nm, 400-600 nm, and 600-800 nm, respectively. The main beam from the predispersing prism forms a spectrum within the instrument. Different sections of this spectrum are then directed toward the four spectral channels of GOME: each channel comprising a grating, transmissive optics and a 1024 element diode array. In this manner the entire spectrum between 232 and 793 nm may be observed: the spectral resolution being ~0.2 and 0.33 nm, below and above 400 nm respectively.

As GOME is optimized for the collection of the upwelling radiation from the atmosphere directly by the scan mirror, it is necessary to direct the extra terrestrial solar output over a diffuser plate to reduce its intensity prior to it being reflected by the scan mirror into the instrument. In this manner both the upwelling radiance and the extraterrestrial irradiance are measured by GOME. The signals, recorded by GOME, are dumped to the ESA ground station at Kiruna. These data are processed for ESA by the GOME Data Processor at the German Atmospheric and Space Research Processing and Archiving Center (DLR-PAC): the resultant level 1 products, TOARAD and ETSIR, and level 2 total ozone column data product are subsequently being distributed to the scientific community.

ERS-2 was launched on the April 20, 1995, into a sun

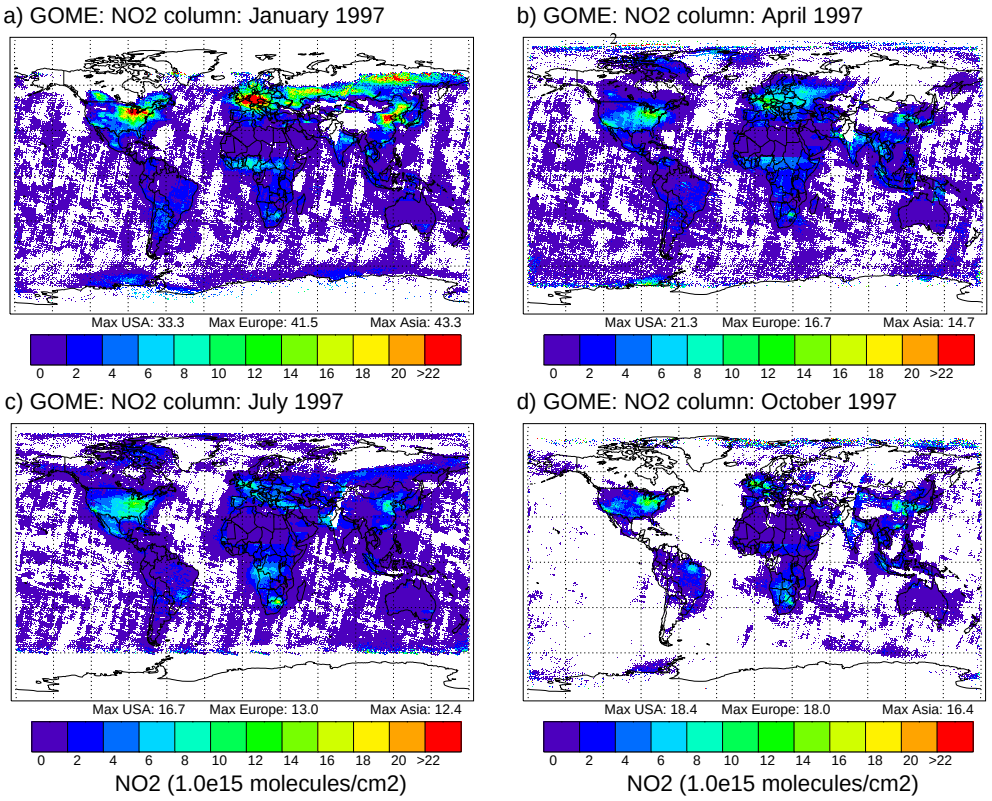

Plate 2. Monthly averaged tropospheric NO_2 columns as derived from GOME measurements for (a) January, (b) April, (c) July, and (d) October 1997. The measurements are made around 1030 LT. The grid shown is 0.45º x 0.45º and derived from both cloudy and cloud free pixels. Blank pixels indicate that there is no data. The maximum values that occur over the United States, Europe, and Asia in a single grid cell are given below the plots. The maximum GOME NO_2 values on the IMAGES grid are (21.9, 30.6, 17.8) for (United States, Europe, Asia) for January, (13.1, 11.0, 6.5) for April, (12.2, 8.7, 7.7) for July, and (12.6, 9.8, 7.9) for October (all in 10^{15} molecules cm^{-2}).

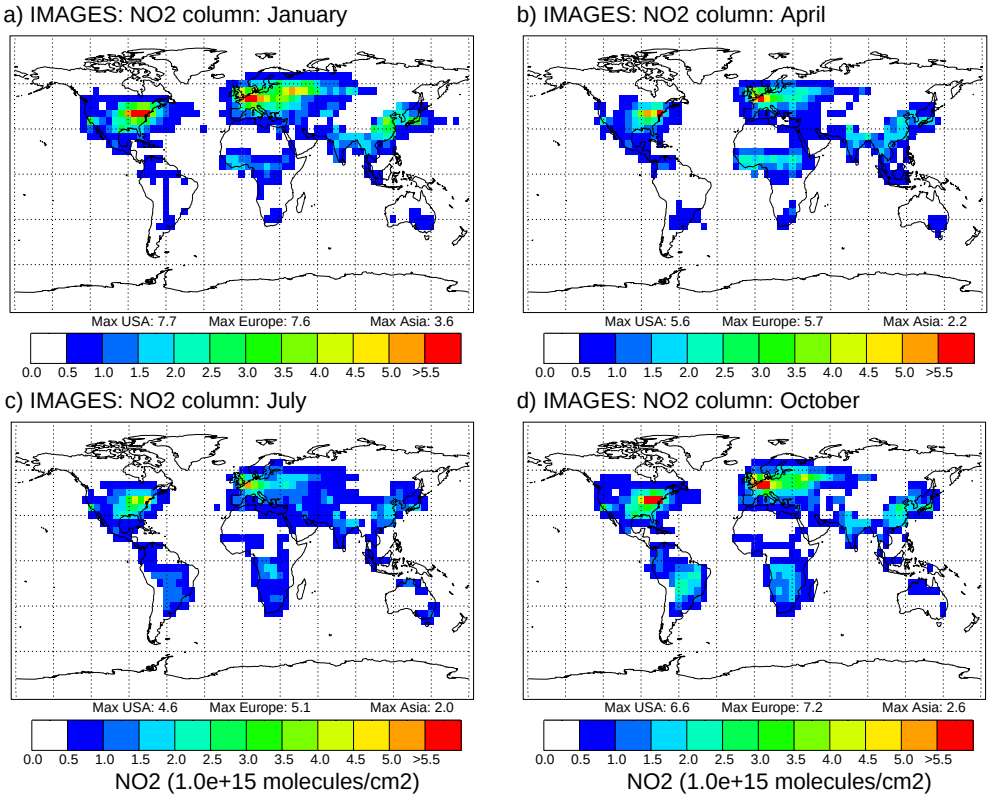

Plate 3. Monthly averaged tropospheric NO_2 columns as calculated by IMAGES for (a) January, (b) April, (c) July, and (d) October. Data correspond to ~1030 LT. The maximum values that occur over the United States, Europe, and Asia in a single grid cell are given below the plots. Note the color scale is 4 times smaller than the scale used for the GOME plots and the lowest level (0-0.5) has been left blank to obtain clearer plots.

synchronous orbit; having an equator crossing time of 10:30 am in a descending node. The scan strategy of GOME yields complete global coverage at the equator in 3 days: the swath width of GOME being 320 x 40 km^2 for the array detector and 20 x 40 km^2 for the PMDs, which are read out 16 times faster than the arrays. More details about the design and the first results from GOME are provided elsewhere [*Burrows et al.*, 1999, and references therein].

2.2. Retrieval Algorithm for Tropospheric NO_2

Using the differential optical absorption spectroscopy (DOAS) technique [e.g., *Platt*, 1994], it has previously been shown that the total column amounts of ozone (O_3) [*Burrows et al*., 1998c] bromine monoxide (BrO) [*Hegels et al.,* 1998; *Richter et al*., 1998; *Wagner and Platt*, 1998], chlorine dioxide (OClO) [*Burrows et al*., 1998c; *Eisinger et al*., 1996; *Wagner et al*., 1999; *Burrows et al.*, 1999], formaldehyde (HCHO) [*Burrows et al*., 1999] sulfur dioxide (SO_2) [*Eisinger and Burrows*, 1998, and references therein], nitrogen dioxide (NO_2) [*Burrows et al*., 1998c; *Leue et al*., 1999], and water vapor (H_2O) [*Noel et al*., 1999] may be retrieved from GOME irradiance and radiance measurements. In addition ozone and aerosol profiles may also be retrieved [*Hoogen et al*., 1999, and references therein].

In this study the DOAS spectral window chosen for NO_2 retrieval from GOME is 425-450 nm [*Wagner*, 1999]. Preflight measurements of the absorption cross section of NO_2, O_3 [*Burrows et al*., 1998a, 1999], H_2O, and O_4 and calculations of an effective Ring spectrum [e.g., *Bussemer*, 1993; *Vountas et al.*, 1998] serve as input for the retrieval. The NO_2 slant column densities derived by DOAS are converted into total atmospheric NO_2 vertical column densities (VCDs) by applying a calculated air mass factor (AMF) for each observation.

The AMF describes the weighted path of the light through the atmosphere compared to the vertical path. In general, the AMF is a function of the solar zenith angle, the selected wavelength interval, the vertical profile of NO_2, amounts of aerosol, the surface spectral reflectance or albedo, the cloud cover, and absorption by the atmosphere. AMFs for this study have been calculated with the radiative transport models AMFTRAN [*Marquard et al*., 2000] for the total atmosphere and GOMETRAN [see *Rozanov et al*., 1997] for the troposphere. The albedo used for AMF calculations in this study are those derived using by cloud free scenes, and an atmospheric model [*Richter and Burrows*, 2000].

In order to retrieve the tropospheric column amounts of NO_2 from GOME data, a priori knowledge about the behavior of the stratospheric NO_2 is required. It is assumed that stratospheric NO_2 is longitudinally homogeneous and the tropospheric NO_2 in the clean remote troposphere above the ocean is negligible. In one approach, known as the tropospheric excess method (TEM) [*Burrows et al.*, 1999], tropospheric NO_2 in the clean remote troposphere over the oceans around 180° longitude is assumed to be negligible. Average three days, weekly, monthly, and yearly global maps can then be derived. In the TEM approach the percentage of cloud cover within a scene is estimated using the higher spatially resolved broad band measurements by a threshold algorithm [*Burrows et al.,* 1998b]. In this manner, composite maps, typically between 60°N and 60°S, showing the tropospheric column of NO_2 for different percentages of clouds can be obtained.

Image-processing techniques (IPT) applied to 3-day composite images of the GOME NO_2 observation has been used extensively in this study. Plate 1 illustrates schematically the individual IPT steps used to discriminate between the stratospheric and tropospheric contribution to the total NO_2 VCDs. For the marine regions the following procedure was used. First, the continents plus a band ~200 km off shore is masked out to avoid regions of NO_2 emissions on and near coastlines. The stratospheric column of NO_2 VCDs is assumed to dominate the resultant region. A normalized convolution is then applied to the data (see *Jähne et al*. [1999] for details), enabling the global stratospheric NO_2 distribution to be inferred. For the IPT algorithm, marine NO_2 measurements for clear sky conditions were selected for which radiative transport calculations can be performed very precisely. For this selection the cloud fraction is derived from the onboard-operated PMD instrument as described by *Wenig et al.* [1999].

Plate 1b shows the "IPT stratospheric background" thus derived. The resulting tropospheric NO_2 VCDs were then obtained from the differences in total atmospheric and inferred stratospheric NO_2 VCDs. A more detailed description of the IPT retrieval of tropospheric NO_2 VCD from the total atmospheric NO_2 can be found in the works of *Leue* [1999], *Leue et al.* [1999, 2001], and *Richter and Burrows* [2000].

In the IPT algorithm, the difference between the total (SCD_{total}) and the stratospheric NO_2 slant column densities (SCD_{strat}) is attributed to tropospheric NO_2. The tropospheric NO_2 VCDs are then computed:

$$VCD_{trop} = (SCD_{total} - SCD_{strat}) / AMF_{trop} .$$

The tropospheric air mass factors (AMF_{trop}) were derived using the radiative transfer model GOMETRAN [*Rozanov et al*., 1997], assuming a well-mixed boundary layer of average height 1.5 km, containing the entire tropospheric NO_2 layer, an average surface albedo being 5%, and a maritime aerosol distribution assumed to be located in the boundary layer.

It should be noted that the results of the IPT algorithm are in good agreement with those of an other approach, known as the tropospheric excess method (TEM) [*Burrows et al.*, 1998c, 1999; *Richter and Burrows*, 2000]. The main difference between TEM and IPT is that in the TEM algorithm cloud free pixels are selected, while in the IPT algorithm all pixels are used and cloud effects are taken into account a posteriori. Because a cloud threshold value is used in the TEM analysis, the residual cloud contamination will lead to an underestimation of tropospheric NO_2.

2.3. GOME's Sensitivity to Boundary Layer NO_2 Observations

The relative penetration of photons in the boundary layer, as observed at the top of the atmosphere, depends strongly on factors including the cloud cover, surface spectral reflectance (albedo), and tropospheric aerosol loading. Thus the weighting of the measurement sensitivity to the lowest levels in the troposphere is a strong function of the wavelength and viewing conditions. This results in a variable sensitivity of the retrieved DOAS NO_2 absorption to the NO_2 in the lowest layer of the atmosphere, the boundary layer. For example, calculations using GOMETRAN show that for cloud free conditions and overhead sun roughly 20% of the incoming solar photons at 437 nm are backscattered by atmospheric molecules before reaching the surface. The backscattering by

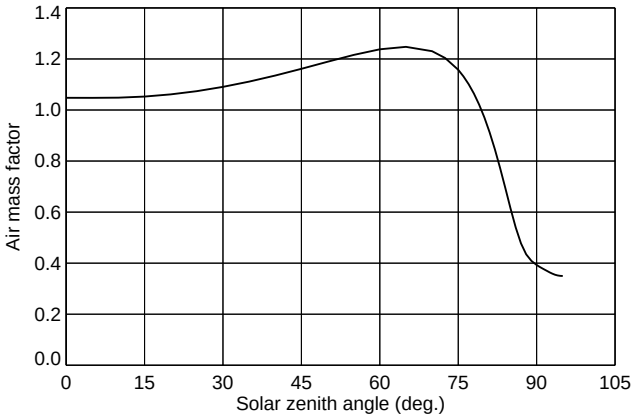

Figure 1. Air mass factor of NO_2 for a boundary layer of 1.5 km at a wavelength of 437.5 nm, assuming an albedo of 5% and a maritime aerosol layer in the boundary layer.

aerosol varies in the range of 1-10% and is dependent on type and distribution. As a result of this sensitivity to the surface spectral reflectance (albedo) in the blue spectral range, ~2-12% of the remaining 80% of the total incoming photons are reflected from nonsnow covered land surfaces, and 4-8% from the oceans [*Richter and Burrows*, 2000]. This behavior is reflected in the air mass factor (Figure 1), which is small and nearly independent of solar zenith angles below 80°.

Our AMF calculations also show that strongly absorbing aerosols located in the boundary layer further obscure the visibility of boundary layer NO_2 for space-borne observations. Multiple Mie scattering by aerosol or cloud particles, however, can also increase the tropospheric absorption due to increasing optical path length. The AMF depends strongly on the surface spectral reflectance, for example increasing the surface spectral reflectance from 4 to 8% increases the tropospheric AMF by ~30%.

Optically thick clouds effectively obscure tropospheric NO_2 located below the cloud top because they act as highly reflecting surfaces, having typically an albedo in the range 80-95% [*Kurosu et al.*, 1997]. As a result of their brightness, even a small cloud fraction within a GOME pixel may contribute significantly to the signal received by the instrument, decreasing the sensitivity toward the detection of boundary layer NO_2, but increasing the relative weighting of NO_2 above the cloud to that of the free troposphere or stratosphere.

2.4. Estimation of the Total NO_2 Column

In this study, in order to estimate the total tropospheric NO_2 VCD all GOME observations (including also the cloudy regions) were taken into account. This procedure enhances the

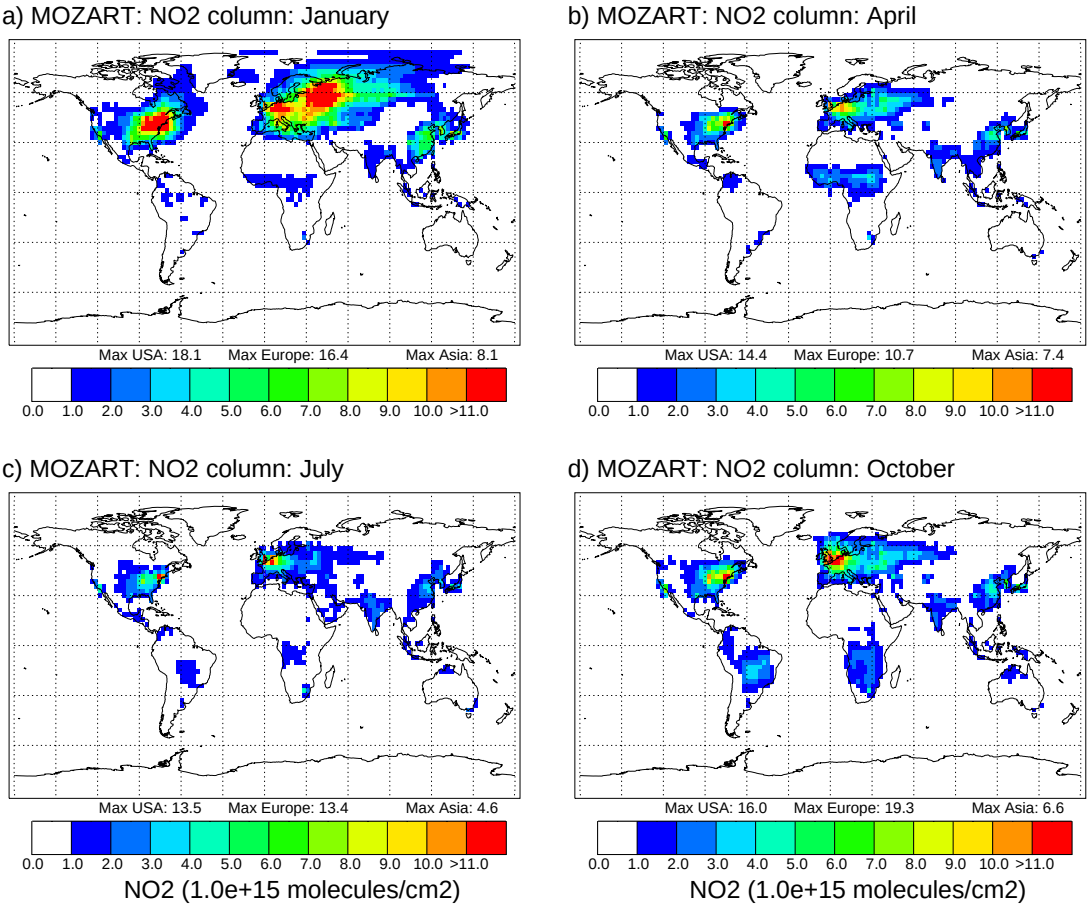

Plate 4. Monthly averaged tropospheric NO_2 columns as calculated by MOZART for (a) January, (b) April, (c) July, and (d) October. Data shown correspond to ~1030 LT. The maximum values that occur over the United States, Europe, and Asia in a single grid cell are given below the plots. Note the color scale is 2 times smaller than the scale used for the GOME plots and the lowest level (0-1) has been left blank to obtain clearer plots.

total number of considered measurements but requires a correction for the effects of clouds on the retrieved tropospheric NO_2. While, in principle, this can be done for individual GOME measurements, we here apply an average correction for monthly averaged GOME measurements of tropospheric NO_2. This approach was chosen in order to reduce the complexity of the correction procedure. In addition, there are still considerable uncertainties in the determination of the individual cloud fractions using current methods.

The average correction applied here makes use of assumptions of cloud fraction and albedo which are described below. They are consistent with conditions over NO_2 source regions, including in particular industrialized regions, but are considered to inappropriate to other regions, e.g., deserts or snow covered regions. Thus the comparisons in this study focus on GOME tropospheric columns of NO_2 and the model results for regions where the above assumptions are valid.

From GOME measurements it turned out that the total atmospheric reflectance (including scattering on the surface, and on aerosols and molecules) is ~25% at 437 nm, whereas the albedo above clouds is equal to or greater than 80%. Thus the geometric cloud fraction has to be weighted by these relative intensities to determine the sensitivity of GOME for the troposphere (assuming that the tropospheric NO_2 column is entirely below the clouds). For a geometric cloud fraction of 0.5 the relative contribution of the clear sky part of the GOME pixel to the total measured signal is ~24%. Thus the respective tropospheric NO_2 column density has to be corrected by about a factor of 4.2. For a geometric cloud fraction of 0.4 (0.6) the relative contribution of the clear sky part to the total signal is ~31% (17%), resulting in correction factor of ~3.2 (5.8). Assuming a Gaussian frequency distribution of the geometric cloud fractions of GOME ground pixels (with a maximum at a cloud fraction of 0.5 and a standard deviation of 0.25), we then derive an average correction factor of about 4 which was applied to tropospheric NO_2 derived by the IPT algorithm, including all the cloudy pixels. No correction factor was applied to the Saharan, Arabian Peninsula, and Australian deserts, since these areas are almost always cloud free.

It should be noted that the assumed frequency distribution of the cloud fractions for GOME ground pixels is somewhat arbitrary but should provide suitable values for many parts of the world (including, e.g., industrialized regions). Future work will yield more precise information on statistics of GOME cloud fractions from improved GOME cloud determination algorithms.

Comparing the TEM NO_2 VCD for all scenes with those having 30% cloud cover, indicates that the TEM NO_2 VCD is typically a factor of 2 larger for the 30% case than over industrial source regions, where the majority of NO_2 is emitted. These findings are in fair agreement with the average cloud correction applied to the NO_2 data derived from the IPT algorithm as described above.

The uncertainty in the tropospheric NO_2 columns from GOME depends mainly on four factors. (1) The precision of the NO_2 DOAS fit, which is limited by photon and electronic noise and can become relatively large for a single observation. Nevertheless, for monthly averaged values this error decreases to very small values (±1%) and can thus be neglected. (2) Systematic errors in the NO_2 DOAS fit (caused, for example, by uncertainties in the wavelength calibration of the reference spectra) do not decrease if several observations are averaged. However, by subtracting the stratospheric column from the total column most of the possible systematic errors cancel out; the remaining systematic error is estimated to be ±10%. (3) The most important uncertainties come from the modeling of the tropospheric AMFs. The lack of precise information about the ground albedo and the tropospheric NO_2 height profile cause errors in the calculated tropospheric NO_2 VCDs which can be up to ~50% for a single observation. For monthly averages these errors partly cancel out leaving an uncertainty of ~15%. (4) The uncertainties caused by clouds constitute the largest contribution to the error. For a single observation it might be up to ~100%. For the monthly averages these errors partly cancel out; we estimate the remaining uncertainty to be ~50%. This last uncertainty dominates the total error in the retrieved tropospheric NO_2 VCDs.

2.5. Monthly Averaged NO_2 Column Amounts for 1997

Plate 2 shows the inferred tropospheric NO_2 columns (=VCDs) for the months of January, April, July, and October in 1997. As expected, the highest NO_2 columns occur over industrialized areas in the Northern America, Europe, and China but hotspots having localized pollution in South Africa, the Arabian Peninsula, and Japan are also clearly discernable. Enhanced tropospheric NO_2 columns also occur in known regions of biomass burning and savannah fires in South America, Africa, and Indonesia (July and October). Much lower NO_2 columns are observed for remote continental regions in Australia or the Sahara desert. The inferred tropospheric NO_2 columns for the remote oceans are close to zero, mainly because for this area the total atmospheric NO_2 column was assumed to be mostly located in the stratosphere (see above). In January the maximum NO_2 columns for the eastern United States, western Europe, and eastern China are twice as large as in the other months; i.e., 33-43 x 10^{15} molecules cm^{-2} versus 14-20· x 10^{15} molecules cm^{-2}. The larger winter values likely result from a decreased loss of NO_2 by reaction with OH (the major NO_x loss process in the lower troposphere), confinement in the boundary layer, reduced vertical transport from the boundary layer to the free troposphere, and slightly increased source strengths.

3. Description of the Models

3.1. IMAGES

The IMAGES model [*Müller and Brasseur*, 1995; *Pham et al*., 1995; *Granier et al*., 1996, 1999, 2000a, 2000b] is a three-dimensional global chemistry transport model that calculates monthly averaged distributions of some 60 species. It has a horizontal resolution of 5º x 5º and includes 25 levels in the vertical extending from the surface to 50 hPa (~22 km). The dynamics is governed by prescribed monthly averaged transport and temperature fields. The distribution of clouds and precipitation rates are also prescribed according to monthly averaged climatological values. The rapid turbulent exchanges in the planetary boundary layer are parameterized using a diffusion coefficient depending on the vertical gradient of potential temperature. The coefficients representing this diffusion coefficient are calculated using monthly mean temperature data.

The chemical scheme in the model is adapted from *Müller and Brasseur* [1995], and its current version is given by

Granier et al. [2000b]. The chemistry includes an explicit description of nonmethane hydrocarbons chemistry including the formation of peroxy-acetyl nitrate (PAN), important for the transport of reactive nitrogen from source regions to the free troposphere [*Moxim et al*., 1996; *Horowitz and Jacob*, 1999]. The reaction rates are from *DeMore et al*. [1997]. The anthropogenic emissions are from the EDGAR emission database [*Olivier et al*., 1996], which is developed in close cooperation with the Global Emissions Inventory Activity (GEIA) of the International Global Atmospheric Chemistry/International Geosphere-Biosphere Programme IGAC/IGBP [see also *Granier et al*., 2000b]. These emissions are specified on a 1º x 1º global resolution for CH_4, NO_x, CO, and nonmethane hydrocarbons. They include emissions from fossil fuel use (industry, transport, fuel production, and transmission), biofuel combustion, industrial processes and solvent use, waste treatment, and agricultural waste burning. A seasonal variation is imposed on the anthropogenic emissions according to *Müller* [1992]. Biomass burning emissions are taken from *Granier et al*. [2000a], based on inventories by *Hao and Liu* [1994]. The production of nitric oxide by lightning discharges is distributed according to the flash frequencies obtained from satellite measurements as reported by *Turman and Edgar* [1982]. Total emission of NO from lightning is assumed to be 5 Tg N/yr.

IMAGES calculates a full diurnal cycle in the first 3 days of the month, with time steps of 1 hour for the first 2 days and a time step of 0.5 hour for the third day. For the rest of the month, diurnal average values are calculated and a time step of 6 hours is used.

3.2. MOZART

The MOZART-2 model is a new version of the model described by *Brasseur et al*. [1998] and *Hauglustaine et al*. [1998]. It is a three-dimensional global chemistry transport model which can calculate the distribution of ~60 species, with a 20 min time step. It has a horizontal resolution of 2.8º x 2.8º and 34 levels in the vertical extending from the surface to 4 hPa (~36 km). The meteorological parameters needed to calculate the advective transport, smaller-scale exchanges, and wet scavenging of long lived chemical species are prescribed and taken from the output of the middle atmosphere version of the National Center of Atmospheric Research (NCAR) community climate model CCM3 and are updated every 6 hours. The parameterization of exchanges in the boundary layer is based on *Holtslag and Boville* [1993] and uses a vertical eddy flux proportional to an eddy diffusion coefficient. The latter depends on a turbulent velocity scale and on the boundary layer height (Richardson number dependent). A countergradient term representing nonlocal transport associated with dry boundary layer convection is also taken into account.

The chemical scheme in the model is the same as the one used in IMAGES [*Granier et al*., 2000b], with reaction rates from *DeMore et al*. [1997]. The emissions of CH_4, CO, NO_x, and hydrocarbons are the same as those used in IMAGES (see section 3.1). The production of NO by lightning is distributed as a function of space and season according to the location of convective clouds as provided by the general circulation model, and the height of the top of convective clouds, as formulated by *Price and Rind* [1992]. As for the IMAGES model, the global production of NO from lightning is assumed to be 5 Tg N/yr. For our calculations only diurnal average concentrations of NO_2 were stored, calculated from the mixing ratios at every 20 min time step. The intermediate data were not saved separately.

4. Modeled NO_2 Column

In the Plates 3 and 4 the modeled tropospheric NO_2 columns (vertical column densities) calculated by the IMAGES and MOZART models (respectively) are shown. Plates 3 and 4 can be compared with Plate 2 showing the GOME NO_2 columns. To obtain a clearer picture, the lowest levels (0-0.5 or 0-1 x 10^{15} molecules cm^{-2}) are left blank. The modeled tropospheric NO_2 columns are obtained from the calculated NO_2 mixing ratios by integrating from the surface to the tropopause.

GOME is in a Sun synchronous orbit. It passes over the equator at 1030 local time (LT) and covers all longitudes at the equator in 3 days. To agree as closely as possible with the local overpass time of GOME, the NO_2 columns as calculated by IMAGES correspond with a local time between 1000 and 1040 LT. They are derived by calculating the ratio of the NO_2 concentration at ~1030 LT and the diurnal average concentrations in the full diurnal cycle of the model. The diurnal average concentration in the middle of the month is then multiplied by this ratio. Details about the difference between the column near 1030 LT and the diurnal average are discussed in section 5 and Plate 7. For the MOZART calculations only diurnal average concentrations of NO_2 were stored, no hourly data. To calculate the NO_2 column amounts from MOZART at the GOME overpass time, we used the results from the IMAGES model to calculate the ratio between the tropospheric NO_2 columns at 1030 LT and the diurnal average columns. This ratio was then used, on a monthly basis, to calculate the columns at 1030 LT for the MOZART calculations.

The NO_x emissions in the model calculations are monthly or yearly averages. Diurnal variations are not taken into account. About 30% of the global NO_x emissions come from road transport. Especially in and around the bigger cities road transport exhibits a strong diurnal variation. During the morning rush hours, larger emissions of NO_x are expected which may affect the NO_2 column at the GOME overpass time (1030 LT). We have performed a calculation with IMAGES using a diurnal variation in the NO_x emissions from road transport according to *Dreher and Harley* [1998]. The effect of a diurnal variation in NO_2 emissions (versus a constant emission) on the tropospheric NO_2 column was found to be small, with very local increases around Los Angeles of ~3%, in the eastern United States 1-5%, northwestern Europe 1-4%, and Japan ~1% (annual averages).

4.1. Grid Sizes and Method of Calculation

Before comparing the modeled NO_2 columns with the GOME measurements, the effect of the different grid sizes has to be considered. In Plates 5a and 5b the GOME NO_2 columns are shown mapped onto the IMAGES and MOZART grids. This smoothes the plots and removes the small very localized spots with high NO_2 columns over industrialized areas. In Plate 5 the corresponding annual averaged modeled NO_2 columns are also shown. In the middle panels the tropospheric columns are calculated by integrating from the surface

to the tropopause, while in the lower panels a similar method as for the GOME columns is applied; i.e., subtracting the NO_2 column over the Pacific (around 180°W) from the NO_2 column at all longitudes. The latter procedure is performed on a monthly basis and retains the latitudinal variation. Comparing both procedures (Plate 5c versus 5e and 5d versus 5f), it can be seen that there is virtually no difference for industrialized areas with large tropospheric NO_2 columns as well as for the more remote continental areas (South America, Africa, and Australia). There are some differences over the oceans, but they are small in an absolute sense. The tropospheric NO_2 columns over the oceans and away from NO_x sources are smaller than 0.5×10^{15} molecules cm^{-2} (middle panels). This is the amount that is subtracted from both the GOME (Plates 5a and 5b) and modeled (Plates 5e and 5f) in the derivation of the tropospheric NO_2 columns but is part of the tropospheric column.

4.2. Comparing Models With GOME

Plates 3 (IMAGES) and 4 (MOZART) can now be compared with Plate 2 (GOME). We must be cautious in making a quantitative comparison, considering the large uncertainties in the retrieval of the tropospheric NO_2 columns from the GOME measurements as discussed above (sections 2.3 and 2.4); these are likely to be as large as 50% for individual locations. A qualitative comparison of GOME with the model calculations is, however, useful, since this uncertainty is likely to affect the NO_2 columns everywhere in a similar manner. Note that Plates 2, 3, and 4 have different scales to show the full range of the NO_2 columns. The figures also differ in the grid sizes (grid size of the GOME data is 0.45° x 0.45°). The magnitude of the NO_2 columns varies greatly in different regions. Because of the color scale chosen, the low NO_2 columns over remote areas are not easily visible in these plates. In Plate 5 the columns from GOME are plotted on the IMAGES and MOZART grids, and the color scale is nonlinear to accentuate the areas with small columns.

The overall picture of the measured tropospheric NO_2 columns is well reproduced by the model calculations: large columns over industrialized areas both in the Northern and Southern Hemispheres, low values over remote continental areas, and very low values over the oceans. Larger tropospheric NO_2 columns are found in winter than in summer, the same as in the GOME observations. The absolute values of the tropospheric NO_2 columns as calculated by MOZART are close to those derived from the GOME measurements, while the column amounts from IMAGES are significantly smaller. The maximum values in IMAGES are about a factor of 2-3 smaller than in GOME for the United States, ~1.5-4 smaller for Europe, and ~3-5 for Asia, using the same grid (that of IMAGES) for both. The maximum values in MOZART are similar to those of GOME for the United States (a factor of 0.8-1.5 smaller) and Europe (0.7-2), but a factor of 1.5-3.5 smaller for Asia (all on the MOZART grid). If averaged over a larger area (subcontinental), the high maximum values in very localized areas in MOZART and in GOME are somewhat reduced. The agreement between the model calculations and the GOME measurements is somewhat worse for South America and Africa, areas with lower NO_2 columns in which biomass burning, savannah fires, and soil emissions are the dominant NO_x sources. Uncertainties in the structure of the boundary layer due to larger convective activity in the tropics may also affect the model values in these regions. The tropospheric NO_2 columns in IMAGES are about a factor of 2-5 smaller than GOME for South America and Africa. The values in MOZART are ~1-2 times smaller for South America and ~3 times for Africa. The modeled columns over the Saharan and Australian deserts are small ($0.2\text{-}0.5 \times 10^{15}$ molecules cm^{-2}).

The following points have to be mentioned in relation to the comparison: (1) The emissions used here correspond with a 1990 inventory and are probably too low for l997, especially for China. *Kato and Akimoto* [1992] found in increase in NO_x emissions in eastern Asia of 4%/yr in the 1970s and 1980s. Extrapolating this trend gives an in increase in NO_x emissions for this area of 32% between 1990 and 1997. This can explain only part of the difference between GOME and MOZART. A larger increase in emissions would be needed to explain the whole difference. (2) Differences for South America and Africa can also be caused by errors in the parameterization of convective processes which transport NO_2 from the boundary layer to higher altitudes. (3) In this comparison we only used one year of GOME data. The NO_2 columns probably display some year-to-year variability, but these real differences are likely to be smaller than the large uncertainties in the GOME tropospheric column amounts and uncertainties in the modeled representation of the boundary layer, suggesting that a better understanding of those factors will be needed before inter annual fluctuations can be meaningfully measured and compared to model calculations.

The differences between the measured and modeled columns can also be seen in Plate 6 where the ratios between the NO_2 column amounts are plotted, i.e., GOME/IMAGES and GOME/MOZART. For calculating these ratios the GOME data have been converted to the IMAGES or the MOZART grid. No ratio is calculated if either the measured or modeled NO_2 column was smaller than 0.1×10^{15} molecules cm^{-2}. Plate 6a shows that for most areas the GOME NO_2 column is 2-3 times larger than the column calculated by IMAGES. Comparing GOME with MOZART (Plate 6b) lower ratios (i.e., better correspondence) are found for the polluted areas; a factor of 0.5-2 for eastern United States and western Europe. The columns measured by GOME over the Sahara and Australia are 1.5-2 times larger than modeled by MOZART. The high ratios around 60°N over western Russia are the result of large NO_2 columns in GOME, probably resulting from an inadequate subtraction of the stratospheric NO_2 column from the total column for these areas.

From these comparisons between the GOME and modeled tropospheric NO_2 columns we conclude that there is a good qualitative agreement between the column amounts retrieved from the GOME measurements and both sets of model calculations. Quantitatively, the GOME columns are of the same order as the ones calculated by MOZART for the polluted industrialized areas.

The results of the IMAGES model differ substantially from those of the MOZART model. This difference is caused mainly by the different representations of the boundary layer and resulting different NO_2 profile in the lowest kilometer of the modeled troposphere in the two models. The MOZART model has a physically more realistic boundary layer with high and more or less homogeneous NO_2 concentrations. In IMAGES the boundary layer cannot maintain a high NO_2 concentration throughout the whole layer. Emitted pollutants are removed too fast from the boundary layer by vertical

diffusion. The boundary layer, which contributes strongly to the total tropospheric NO_2 column in polluted areas, therefore contains less NO_2 in IMAGES than in MOZART (see also section 6).

5. Contributions to the NO_2 Column

Now that we have considered the modeled tropospheric NO_2 columns in section 4, we probe the build up of the NO_2 column, some aspects of the chemical partitioning, and the contributions from different vertical layers based on model calculations only.

5.1. NO_x and NO_y

As mentioned above, GOME passes over the equator at 1030 LT, so it performs its measurements at various latitudes between ~10 and ~11 LT. In Plate 7a the difference in tropospheric NO_2 column at ~1030 LT and the diurnal average column is given as a ratio as calculated by IMAGES. Over industrial areas in the eastern United States and western Europe the tropospheric NO_2 column at the GOME overpass time is ~80% of the diurnal average column. Over South America and Africa it is slightly less, 50-70%. Any errors in the diurnal partitioning of NO_2 are therefore likely to be too small to substantially affect the comparison between GOME and the model calculations.

In the atmosphere, NO and NO_2 exhibit a clear diurnal variation: during the day NO_2 is converted to NO by photolysis, while during the night NO is converted back into NO_2 mainly by the reaction with ozone. The sum of NO and NO_2 (=NO_x) remains more or less constant during this cycle. The annual average lifetime of NO_x in the IMAGES troposphere is ~12 hours, while it is ~7 hours in the lowest 5 km of the Northern Hemisphere between 20°N and 70°N. It is interesting to see how large the tropospheric NO_2 column is compared with the tropospheric NO_x column. An error in the modeled NO_2/NO_x ratio could alter the comparison with GOME measurements. This ratio, yearly averaged, is shown in Plate 7b and 7c. In IMAGES (Plate 7b) the NO_2 column is 60-70% of the NO_x column over the continents (diurnal and annual average) with maximum values of ~80% for the eastern United States, western Europe, and eastern China. The NO_2/NO_x ratio for MOZART (Plate 7c) is overall slightly higher. Over the most polluted areas ratios of ~60% are found. These lower ratios are most pronounced in the winter months with values as low as 30%, while in summer, there is no difference over the United States and Europe (ratio ~80%). The lower NO_2 and higher NO values in winter are probably the result of direct NO emissions, slower photolysis of NO_2 to NO, and reduced conversion of NO to NO_2 because of lower ozone concentrations. This effect is not observable in the IMAGES model, probably because of the diffusive nature of the boundary layer, which transports NO and NO_2 upward out off the boundary layer too rapidly. An error in the NO_2/NO_x ratio could affect the agreement with the GOME measurements, although the modeled ratio is close to the observed ratio of ~80-90% in the boundary layer in eastern North America in August [*Parrish et al*., 1993].

Assuming the total NO_x emissions are relatively well known, the tropospheric NO_2 column in the model calculations can also be affected by a different distribution of nitrogen species between NO_2 (or NO_x) and NO_y. The NO_y species with the largest tropospheric column is HNO_3, with ~10-18 x 10^{15} molecules cm^{-2} over the industrialized areas for both IMAGES and MOZART. The NO_x/NO_y ratio over the industrialized areas in the United States and Europe is ~20-40% in IMAGES and 30-70% in MOZART. The observed NO_x/NO_y ratio [*Parrish et al*., 1993] ranges from ~30 to ~50% at daytime and from ~50 to ~70% diurnally averaged in eastern North America in August. The MOZART values are in better general agreement with these observations than the IMAGES values. The models differ on their treatment of the nitrogen species resulting in different NO_x/HNO_3 ratios. This difference is mainly caused by a different wet deposition of HNO_3 and does not affect the NO_x concentration in the model very much [*Velders and Granier*, 2001]. With respect to the column, the middle and upper troposphere contribute more to the HNO_3 tropospheric column than in the case of NO_2, but the lower troposphere and boundary layer dominate the column for both species over industrialized areas. The large NO_y column and uncertainty in it shows that the modeled NO_2 columns could be substantially affected by errors in this partitioning (see section 6).

5.2. Contribution of Different Layers

In section 5.1 and in section 4 we have considered the whole tropospheric column of NO_2. Now we will consider the contributions of different layers to the total tropospheric column, focusing in particular to how sensitive the total tropospheric column is to the boundary layer. In Plate 8 the NO_2 column in shown integrated up to the tropopause but starting at layer 1 (surface), layer 2 (bottom at 0.17 km), layer 3 (0.45 km), and layer 4 (0.94 km) as calculated by the MOZART model. From these plots it can be seen that over the more polluted continental areas the first three layers individually contribute more to the total tropospheric NO_2 column than all other layers combined. Over the industrialized areas in the eastern United States and western Europe layer 1 makes up 25-40% of the total tropospheric NO_2 column, layer 2 another 25-40%, layer 3 ~15-25%, and the other layers combined yield 10-20%. Over the remote continental areas of South America and Africa the first layer contributes 15-25%, the second layer 10-20%, the third 5-15%, while the other layers contribute 40-70%. Over the remote oceans, i.e., away from the continents, the layers above 1 km altitude contribute more than 97% to the total tropospheric column. Closer to the continents and in the North Atlantic the layers above 1 km contribute 80-90% to the total column.

The lowest few layers, representing the boundary layer, in the MOZART model clearly contribute most to the tropospheric NO_2 column (the same holds for IMAGES). The boundary layer is difficult to model properly in a global atmospheric model, since the chemical and dynamical processes in the boundary layer occur on spatial and temporal scales that are too small for the relatively coarse spatial resolution and time step of global models. Therefore, on a local scale of tens of kilometers much higher NO_2 concentrations might be found in the boundary layer than calculated by global models, which can increase the tropospheric NO_2 column significantly. As has been shown in section 2.3, GOME's sensitivity to NO_2 in the boundary layer is a complex function of albedo and wavelength, resulting in a large uncertainty in the derived tropospheric columns.

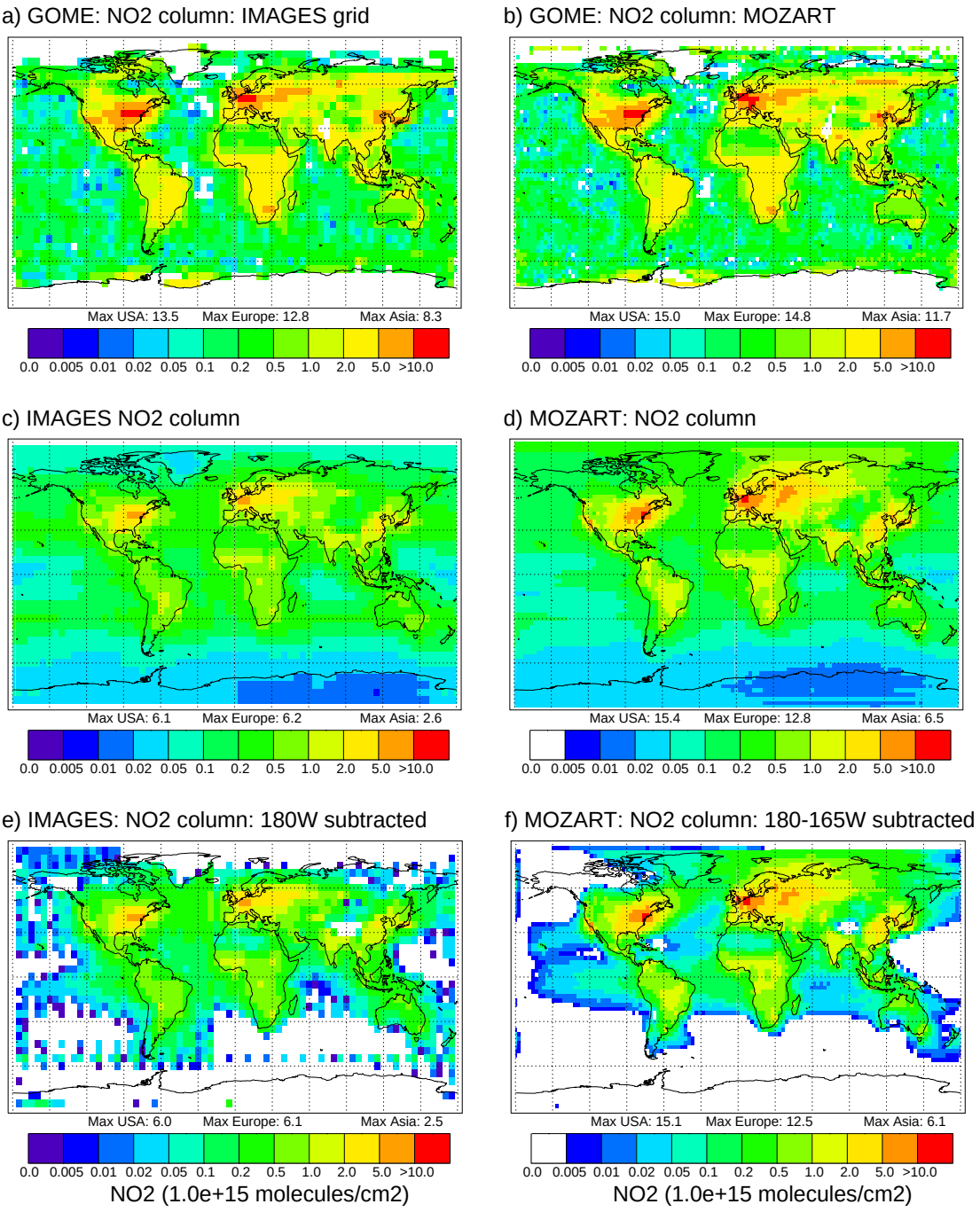

Plate 5. Yearly averaged tropospheric NO_2 columns of GOME (a, b), IMAGES (c, e), and MOZART (d, f): all plotted on (left) the IMAGES grid of 5° x 5° and (right) the MOZART grid of 2.8° x 2.8°. (c) and (d) the tropospheric column is calculated by a summation from the surface to the tropopause, while in (e) and (f) the tropospheric column is calculated by subtracting a longitude band over the Pacific from all longitudes. The latter method is similar to what is used to derive the tropospheric column from the total column in the GOME data. The columns correspond to ~1030 LT. Note a nonlinear color scale is used.

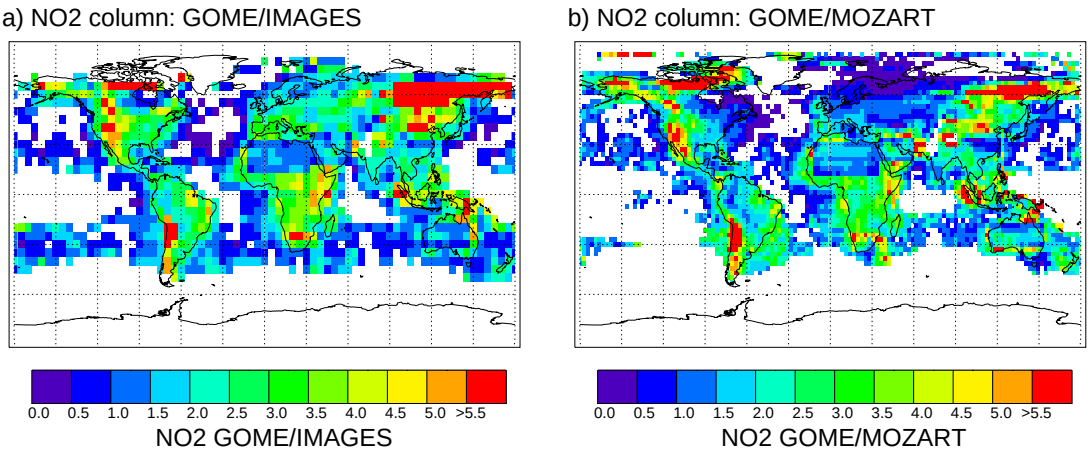

Plate 6. Ratios of the NO_2 columns from GOME relative to the IMAGES and MOZART columns, i.e., (a) GOME/IMAGES and (b) GOME/MOZART. Shown are (as a fraction) the yearly averaged columns corresponding with 1030 LT. The ratio is only plotted if both the GOME and model derived NO_2 columns are larger than 0.1 x 10^{15} molecules cm^{-2}.

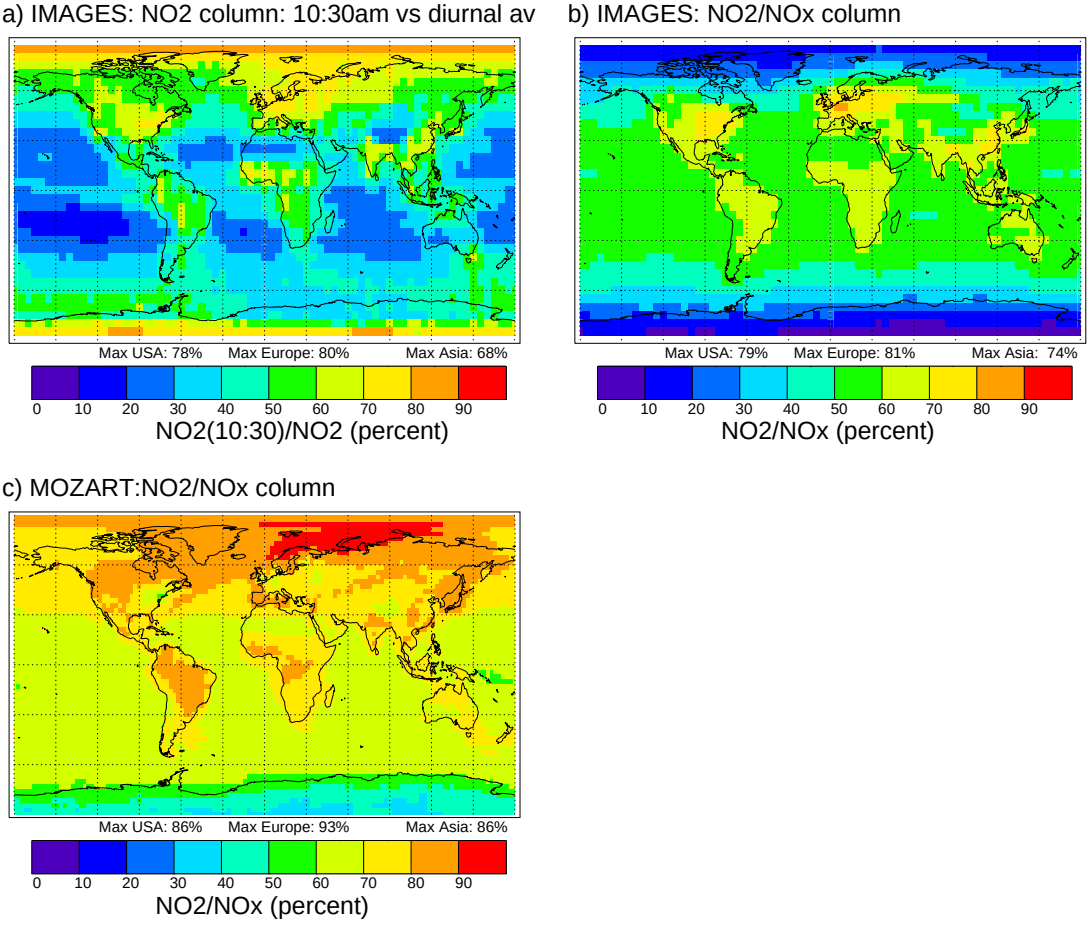

Plate 7. Ratios between (a) the tropospheric NO_2 column at 1030 LT and the diurnal average column (IMAGES), and between the diurnal average tropospheric NO_2 column and the NO_x column calculated by (b) IMAGES and (c) MOZART. Yearly averaged columns are shown.

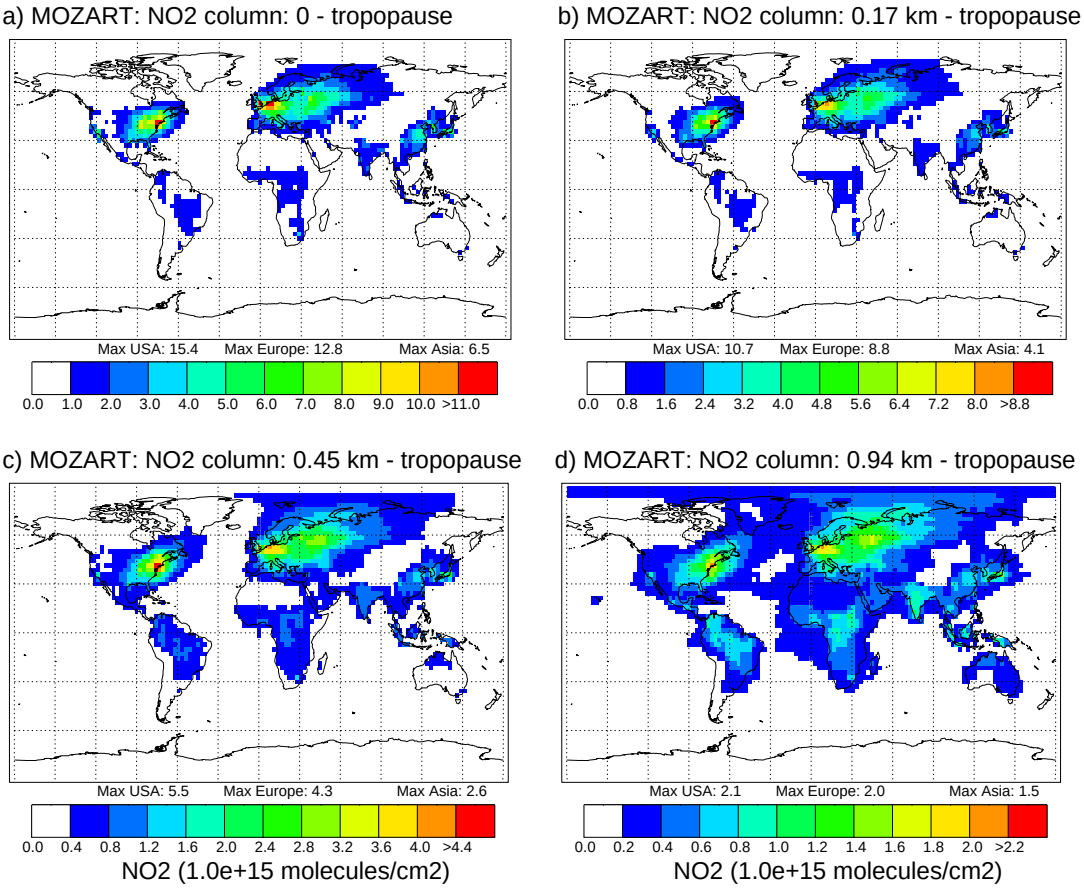

Plate 8. Different vertical integrations for calculating the yearly averaged tropospheric NO_2 column as calculated by MOZART (1030 LT). The integrations are performed up to the tropopause but starting at, (a) the surface, (b) 0.17 km, (c) 0.45 km, and (d) 0.94 km.

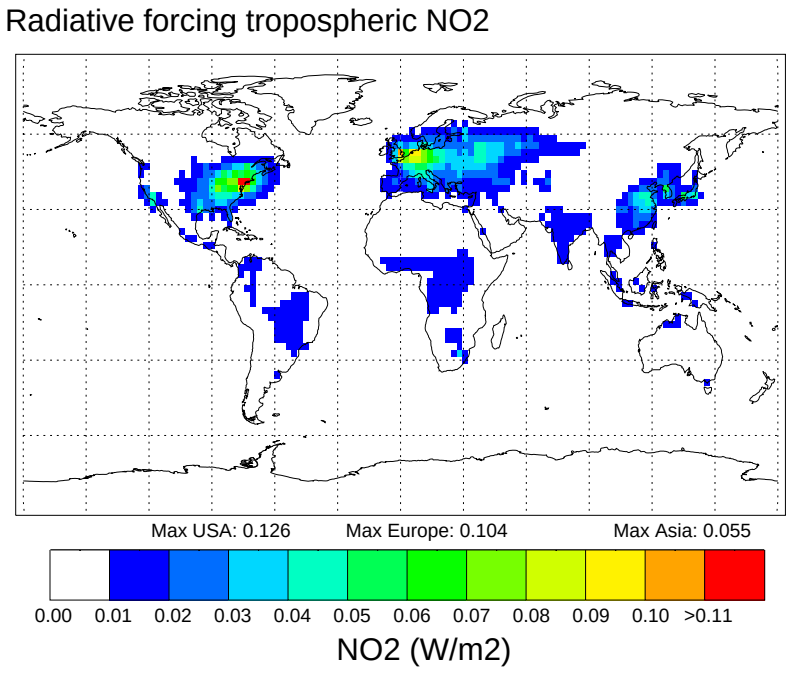

Plate 9. Annual average radiative forcing (W m^{-2}) of tropospheric NO_2 calculated with MOZART. The radiative forcings are diurnal averages for cloud free conditions, calculated using the daytime average tropospheric NO_2 columns.

5.3. Heterogeneous Conversion of HNO_3 on Soot

Lary et al. [1997] proposed that a heterogeneous conversion of HNO_3 to NO might take place on soot. This reaction can increase the NO and thereby NO_2 concentrations in the troposphere. It has its largest affect over and downwind of polluted areas where large concentrations of both HNO_3 and soot occur, i.e., the east of China, eastern Europe, and Siberia, with smaller effects in the eastern United States and during the biomass burning season in the tropics over South America and Africa and downwind from there. *Hauglustaine et al*. [1996] showed that this reaction could reduce the HNO_3/NO_x ratio in the free troposphere at Hawaii, rendering modeled values in better agreement with measurements.

The effect of this reaction on the tropospheric NO_2 column was studied using IMAGES. Since soot is not explicitly modeled by IMAGES, it was crudely represented as sulfate (SO_4) in the calculations. This is intended only to test how sensitive the NO_2 columns are to a possible heterogeneous conversion of HNO_3. Soot and sulfate have similar sources and distributions and the reaction rate is adjusted to account for the difference in absolute values between soot and sulfate. A reaction rate of 0.3 x 10^{-15} $cm^{-3}s^{-1}$ was used, which is equivalent to a conversion lifetime of 2 days in the Northern Hemisphere, 0-5 km altitude. This results in tropospheric NO_2 columns in the eastern United States and western Europe of ~10 x 10^{15} molecules cm^{-2}, an increase of 20-30%. Larger increases occur over western Russia (80-120%), Siberia (more than 80%), and eastern China (60-80%). This heterogeneous conversion of HNO_3 has little effect in the Southern Hemisphere. Thus reactions on soot may significantly increase the modeled NO_2 column amounts.

6. Validation of Tropospheric NO_2

In the previous sections we have compared the tropospheric NO_2 columns from GOME with column amounts from chemistry transport models and found differences in the absolute values of the columns. In this section the focus is on the validation of the GOME NO_2 values. Obviously, the most straightforward way to validate NO_2 columns from GOME is to compare them with column measurements made from the ground. A large number of NO_2 column measurements from ground based stations is available but they mostly focus on stratospheric NO_2 and are in remote locations or on mountain tops (e.g., data from the Network for Detection of Stratospheric Change, NDSC). The focus in this study is on NO_2 in the polluted areas of United States, Europe, and Asia with only a few (or none at all) systematic NO_2 column measurements at these locations. We therefore compare modeled NO_2 mixing ratios with measurements in the boundary layer to assess indirectly the quality of the modeled NO_2 columns. Using the comparisons between GOME and the model calculations in the sections 4 and 5 we can then get an idea of the quality of the GOME measurements. We also compare tropospheric NO_2 columns from GOME and the models with columns inferred from mixing ratio measurements in the boundary layer.

Local measurements of NO_2 in the boundary layer are performed by many institutes all over the world. They generally take place in cities for local air quality studies. The *EPA* [1998] performs measurements of NO_2 at various surface locations in the United States on a daily basis. They report yearly average NO_2 levels at urban sites of ~24 ppbv, suburban sites of ~20 ppbv and at rural sites of ~8 ppbv for the 1990s. Their chemiluminescence measuring technique is sensitive not only to NO_2 but also to other nitrogen-containing compounds such as PAN. This can cause an overestimation of the reported NO_2 levels, especially in rural areas [*EPA*, 1998]. These data are therefore less useful for our study, but they do show that very high mixing ratios are found in polluted areas, in agreement with very large local NO_2 columns over industrialized areas. Measurements in the free troposphere [e.g., *Emmons et al*., 2000] are also less relevant for this study since the free troposphere contributes only a small amount to the tropospheric NO_2 columns.

Measurements of reactive nitrogen at rural ground sites in eastern North America were reported by *Parrish et al*. [1993]. In late summer of 1988 they measured several tropospheric trace species, including NO, NO_2, and NO_y at seven surface locations representative for rural areas in the populated regions of eastern North America. Mixing ratios over rural areas in industrialized regions of the United States and Europe are best suited for validating the GOME and modeled data, considering the grid sizes of GOME and of the models used here. *Parrish et al*. [1993] found that the daytime (1000-1800) median NO_y levels for a fully convective well mixed boundary layer were 2 to 5 ppbv. The NO_y levels vary at each site by an order of magnitude or more. The daytime NO_x/NO_y ratio was 30-50%. The observed daytime NO/NO_y ratio was ~5%. From this we derive NO_2 daytime values ranging from 0.5 to 2.2 ppbv. The diurnal average NO_2 values are ~1.1-2.8 ppbv and ~1.3-3.2 ppbv at the GOME overpass time of 1030 LT.

In Figure 2 the modeled diurnal average NO_2 mixing ratios in the boundary layer are shown for the United States in August. These mixing ratios broadly agree with other model calculations [*Levy et al*., 1999; *Horowitz and Jacob*, 1999] which show boundary layer values above 1 ppbv over the industrialized areas. The NO_2 measurements [*Parrish et al*., 1993] are representative for a well-mixed boundary layer. The lowest layers in the model calculations do not show a uniform mixing ratio but have high values close to the surface and decreasing towards the top of the boundary layer. For the comparison the modeled mixing ratios are averaged over the lowest eight model layers for IMAGES (0-1.4 km) and the lowest four model layers for MOZART (0-1.6 km). The calculated average values for the eastern United States are 0.7-1.0 ppbv for IMAGES and 1-3 ppbv for MOZART. The latter values agree well with the measured values (0.5-2.2 ppbv), but those of IMAGES are too low. In the lowest layer in the models, NO_2 values are as high as 4 ppbv (IMAGES) and 15 ppbv (MOZART). In winter, with a smaller boundary layer, values more than twice as large are found both for the average in the boundary layer and in the lowest layer.

A mixing ratio of 1 ppbv in a well mixed boundary layer of 1 km contributes 2.69 x 10^{15} molecules cm^{-2} to the total column. The observed 1.3-3.2 ppbv of NO_2 at ~1030 LT therefore yields ~3.5-8.6 x 10^{15} molecules cm^{-2} for a boundary layer of 1 km. Adding to this an NO_2 column in the free troposphere of ~1.5 x 10^{15} molecules cm^{-2} (August data from MOZART model), we obtain a total tropospheric column of 5.0-10.1 x 10^{15} molecules cm^{-2}. The NO_2 columns retrieved from GOME in the eastern United States in August are ~7-10 x 10^{15} molecules cm^{-2}, with maximum values up to 16 x 10^{15} molecules cm^{-2} in very localized areas. This is within the

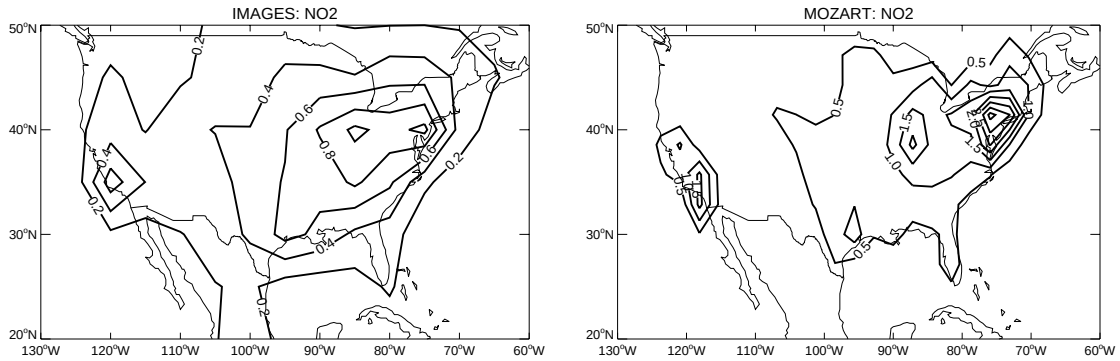

Figure 2. Diurnal average NO_2 mixing ratios (ppbv) in the boundary layer for August calculated with (a) IMAGES and (b) MOZART. The mixing ratios are averaged over the lowest 1.5 km of the modeled atmosphere.

range of the columns inferred from the measured NO_2 mixing ratios and slightly larger than the columns calculated with the MOZART model (4-8 x 10^{15} molecules cm^{-2} at ~1030 LT in August, with a local maximum of 13 x 10^{15} molecules cm^{-2}). The values from IMAGES are 2.5-4.2 x 10^{15} molecules cm^{-2}.

The following qualifications concerning this comparison need to be taken into account:

1. The boundary layer thickness is not known exactly, affecting the comparison of the modeled columns with the surface mixing ratio data. The thickness of 1 km we assumed here is probably on the low end, resulting in a low estimate of the column inferred from the surface mixing ratios.

2. The boundary layer in the model calculations does not have a uniform mixing ratio but exhibits high surface values decreasing toward the top of the boundary layer. For this comparison, the average of the mixing ratios in the lowest 1.5 km has been used. This is not necessarily the same as a well-mixed boundary layer because of possible nonlinear NO_x chemistry.

3. The relatively large grid size of the models affects the NO_x chemistry since the NO emissions are emitted into these boxes and diluted more than in reality, resulting in lower local concentrations and a different conversion to NO_2.

4. High NO_2 mixing ratios and columns occur on a local scale in urban and suburban areas (see large mixing ratio in urban and suburban areas as measured by the *EPA* [1998]), which cannot be modeled in a global model and probably difficult to observe by GOME, but can affect the NO_2 columns from both.

5. The data (GOME, model, and surface NO_2 mixing ratios) all show considerable spatial variability, which complicates the comparison.

These considerations do not change the overall picture that the tropospheric NO_2 columns from GOME over eastern North America are of the same order as those derived from both the observed in situ NO_2 mixing ratios and those from the model calculations with MOZART.

7. Radiative Forcing of Tropospheric NO_2

In addition to playing a role in the formation of ozone in the troposphere, NO_2 also absorbs solar radiation and thereby may contribute to the radiative forcing of climate. *Solomon et al*. [1999] showed that over Boulder (Colorado) NO_2 can cause a local instantaneous absorption of radiation in the troposphere of up to ~2-10 W m^{-2}, likely resulting from air pollution. Over polluted areas in the eastern United States, northwestern Europe, and the east of China a larger local radiative absorption can be expected. Absorption of solar radiation in the troposphere by NO_2 of up to 30 W m^{-2} has been estimated to take place in clouds during thunderstorms [*Solomon et al*., 1999]. Note that the local radiative absorption values given by *Solomon et al*. [1999] correspond to the net absorption occurring in the tropospheric air column. This is different from the radiative climate forcing (i.e., the change in flux at the tropopause) since it includes absorption which would have occurred at the ground anyway. The difference is largest for clear skies and cloudy skies where the absorber is located below the cloud (for optically thick clouds where the absorber is located in or above the cloud the difference is relatively small). In this section we use the modeled NO_2 columns from IMAGES and MOZART to make a global map of the radiative forcing by NO_2 in the troposphere for clear sky conditions.

A line-by-line radiative transfer calculation which incorporates the DISORT [*Stamnes et al.*, 1988] scattering code has been used in this study. This is the same basic model as used in *Solomon et al.* [1999]. A perturbation profile of NO_2 with all of the NO_2 in the lowest 1 km is assumed since the models show that most of the NO_2 is in the boundary layer in polluted regions. Overlap with O_3 and O_4 is included although their influence is small except for O_3 absorption in the UV. A ground albedo of 0.05 is assumed, which is reasonable for continental urban areas in the blue region of the spectrum. An aerosol layer is included in the boundary layer with an optical depth of 0.1, a single scattering albedo 0.85, and an asymmetry factor of 0.7, which are very con-servative estimates for polluted regions. The diurnal cycle is integrated over for the 15th day of each month as a function of latitude for clear sky conditions. This yields a local radiative forcing efficiency per NO_2 molecule (W m^{-2}/cm^{-2}) which can be multiplied by the NO_2 column to obtain the local radiative forcing.

Plate 9 shows the diurnal annual average radiative forcing of tropospheric NO_2 as calculated using the daytime averaged tropospheric NO_2 columns from MOZART. Since the daytime NO_2 columns were not directly available from the MOZART calculations, we used the results from the IMAGES model to calculate the ratio between the daytime average tropospheric

NO_2 columns and the diurnal average columns. This ratio was then used on a monthly basis to calculate the daytime average columns for the MOZART calculations. The maximum monthly values attained by the local radiative forcing of tropospheric NO_2 are 0.1-0.15 W m^{-2}. Much larger values can be expected in cities where very high NO_2 concentrations are observed; events that are not well represented in the global model calculation presented here. These local "hot spots" over industrialized areas could be important for local heating in urban areas. On a more continental scale a radiative forcing of 0.04-0.1 W m^{-2} is calculated over the eastern United States, western Europe, and eastern Russia. The calculation of radiative forcing illustrates the regional distribution and magnitude, at least to a factor of 2 accuracy. The calculated values are of the same order as the radiative forcing of the well-mixed greenhouse gas N_2O (0.14 W m^{-2}) but smaller than the radiative forcing of the halocarbons (0.25 W m^{-2}) and of tropospheric ozone (0.2-0.6 W m^{-2}) [*Intergovernmental Panel on Climate Change*, 1996; *Kiehl et al*., 1999; *World Meteorological Organization*, 1999]. Globally averaged, the estimated radiative forcing of tropospheric NO_2 is relatively small having a value of ~0.005 W m^{-2}. The radiative forcing of NO_2 shows a small seasonal cycle, with ~15% larger values than average in winter/spring and ~15% lower values in autumn. The seasonal cycle is not very large because the larger forcing in the summer compared with the winter, due to the zenith angle dependence, is compensated by the smaller NO_2 columns. Assuming a larger ground albedo of 0.15 in the calculation increases the estimated radiative forcing by a factor of 2. Forcing maps derived from the IMAGES calculations are about half those derived from MOZART.

The radiative forcing of tropospheric NO_2 as estimated here is based on cloud free conditions. Since the bulk of the NO_2 resides in the boundary layer below the clouds, clouds effectively shield the solar radiation from the NO_2. Even clouds with relatively small optical depths will reduce the globally averaged radiative forcing. For example, a cloud with an optical depth of 10 will reduce the radiative forcing by 65%. Thus, as a lower limit we can assume that clouds will reduce the estimated local radiative forcing by nearly the fraction of local cloud cover. Assuming an average cloud cover of 50% the maxima in the local radiative forcing over the industrialized areas becomes ~0.05-0.08 W m^{-2}.

8. Conclusions

Tropospheric NO_2 columns derived from GOME data have been compared with that from model calculations by two global three-dimensional chemistry transport models, IMAGES and MOZART. The global patterns in NO_2 columns are well reproduced by the models: large tropospheric columns over the industrialized areas of the eastern United States, Europe, and Asia, as well as over cities in Africa and South America; increased NO_2 columns are found over the biomass burning areas of Africa and South America. The variation through the seasons is also similar in both the GOME and the model data sets, having larger values in winter and smaller ones in summer. The quantitative comparison is limited by the uncertainty in the tropospheric NO_2 columns derived from GOME caused by the uncertainty in the air mass factors and cloud cover and due to the difficulty of modeling the dynamics of the boundary layer properly in global models. A tentative comparison of the absolute values shows that the measured tropospheric column amounts inferred from GOME are of the same order as those calculated by MOZART over industrialized areas. The maximum values in MOZART are similar to those of GOME for the United States (a factor of 0.8-1.5 smaller) and Europe (0.7-2), but a factor of 1.5-3.5 smaller for Asia (on the same grid). If averaged over a larger area (subcontinental) the high maximum values in very localized areas in MOZART and in GOME are somewhat reduced. The agreement between the model calculations and the GOME measurements is somewhat worse for South America and Africa, areas with lower NO_2 columns in which biomass burning, savannah fires, and soil emissions are the dominant NO_x sources. The maximum values of IMAGES are significantly smaller than those of GOME: about a factor of 2-3 for the United States, ~1.5-4 for Europe, and ~3-5 for Asia, using the same grid for both.

Over polluted areas the largest contribution to the tropospheric NO_2 column originates from the boundary layer. The boundary layer is difficult to model properly in a global atmospheric model, because the chemical and dynamical processes in the boundary layer occur on spatial and temporal scales that are too small for the relatively coarse spatial resolution and time step of global models. Therefore much higher NO_2 concentrations might be found on smaller scales (several kilometers) in the boundary layer than those calculated by global models, which can locally increase the tropospheric NO_2 column significantly.

The effect of a possible heterogeneous conversion (on soot) of HNO_3 to NO on the modeled NO_2 columns in the troposphere has been studies with the IMAGES model. We found that this reaction can increase the modeled tropospheric NO_2 columns with 20-30% in the eastern United States and western Europe and around 100% in western Russia, Siberia, and eastern of China. The modeled ratios NO_2/NO_x and NO_x/NO_y have been analyzed and found to be close to observations over eastern North America, adding confidence to model calculations of the NO_2 columns.

The modeled tropospheric NO_2 columns from MOZART as well as the columns measured by GOME agree with NO_2 columns derived from observed NO_2 mixing ratios in the boundary layer in eastern North America: the NO_2 columns from GOME are 7-10 x 10^{15} molecules cm^{-2}, from MOZART are 4-8 x 10^{15} molecules cm^{-2}, and those derived from the surface mixing ratios are 5-10 x 10^{15} molecules cm^{-2}. In IMAGES, NO_2 is transported out of the boundary layer too fast resulting in lower NO_2 columns (2.5-4 x 10^{15} molecules cm^{-2}). Qualitatively, the pattern of tropospheric NO_2 columns as measured by GOME agree well with the ones calculated by MOZART and IMAGES. A quantitative comparison is more difficult, but indicates that the GOME NO_2 columns, those calculated by MOZART, and those derived surface mixing ratios are all of the same order for eastern North America.

An estimate of the radiative forcing of NO_2 has been made using the calculated tropospheric NO_2 columns from MOZART. The local maxima over the eastern United States and western Europe in the radiative forcing of tropospheric NO_2 is 0.1-0.15 W m^{-2}, while values of 0.04-0.1 W m^{-2} are estimated on a continental scale (cloud free conditions). The all sky estimates are about a factor of 2 smaller than the clear sky values. These values are of the same order as the radiative forcing of N_2O but smaller than that of the halocarbons and tropospheric ozone. The globally averaged radiative forcing is negligible, ~0.005 W m^{-2}.

Acknowledgments. We would like to thank M. Buchwitz, R. Harley, D. Parrish, V. Rozanov, S. Solomon, and M. Trainer for useful discussions and support in the work and J.-F. Müller for his help with the IMAGES model. Part of the work was performed while one of the authors (K. Pfeilsticker) held a National Research Council-NOAA Research Associateship. J. Burrows and A. Richter acknowledge funding by the University of Bremen, the German Ministry for Education and Research (BMBF) and the European Commission. Part of this work has also been supported by the European Commission under the POET project (contract EVK2-1999-00011). Some simulations have been performed using computer time provided by the National Center for Atmospheric Research (NCAR), which is sponsored by the National Science Foundation.

References

Bovesmann H., J. P. Burrows, M. Buchwitz, J. Frerick, S. Noël, V. V. Rozanov, K. V. Chance, and A. P. H. Goede, SCIAMACHY - Mission objectives and measurement modes, *J. Atmos. Sci., 56*, 126-150, 1999.

Brasseur, G. P., D. A. Hauglustaine, S. Walters, P. J. Rasch, J.-F. Müller, C. Granier, and X.-X. Tie, MOZART: A global chemical transport model for ozone and related chemical tracers, 1, Model description, *J. Geophys. Res. 103*, 28,265-28,289, 1998.

Burrows J. P., W. Schneider, and K. V. Chance, 'GOME and SCIAMACHY: Remote sensing of stratospheric and tropospheric trace gases, in *CEC Air Pollution Research Report 34: Polar Stratospheric Ozone Proceedings of the First European Workshop, 3-5 October 1990 Schliersee, Baveria Germany,* edited by J. A. Pyle and N. R. P. Harris, pp. 99-102, Office for Publ. European Communities, Luxembourg, 1991.

Burrows, J. P., et al., Global Ozone Monitoring Experiment, Interim Science Report, Eur. Space Agency Spec. Publ., ESA SP-1151, 1993.

Burrows, J. P., A. Dehn, B. Deters, S. Himmelmann, A. Richter, S. Voigt, and J. Orphal, Atmospheric remote sensing reference data from GOME, 1, Temperature dependent absorption cross section of NO_2 in the 231-794 nm range, *J. Quant. Spectr. Radiat. Trans.*, *60*, 1025-1031, 1998a.

Burrows J. P., T. Kurosu, R. Guzzi, E. Cattani, M. Cattani, M. Cervino, Ch. Levoni, and F. Torricella, GOME cloud and aerosol data products algorithm development, final report contract 11572/95/NL/CN, Eur. Space Agency, Noordwijk, Netherlands, 1998b.

Burrows, J. P., M. Buchwitz, M. Eisinger, V. Rozanov, M. Weber, A. Richter, and A. Ladstätter-Weißenmayer, The Global Ozone Monitoring Experiment (GOME), mission, instrument concept, and first scientific results, in *Proceedings of the Third ERS Symposium Florence 18th-23rd of March 1997, Space at the Service of our Environment, Eur. Space Agency Spec. Publ., ESA SP 414,* 585-590, 1998c.

Burrows, J. P., et al., The Global Ozone Monitoring Experiment (GOME): Mission concept and first scientific results, *J. Atmos. Sci.*, *56*, 151-175, 1999.

Bussemer, M., Der Ring-Effekt: Ursachen und Einfluß auf die spektroskopische Messung stratosphärischer Spurenstoffe, Diploma thesis, Univ. of Heidelberg, Heidelberg, Germany, 1993.

Chameides, W. L., et al., Ozone precursor relationships in the ambient atmosphere, *J. Geophys. Res.*, *97*, 6037-6055, 1992.

DeMore, W. B., D. M. Golden, R. F. Hampson, C. J. Howard, C. E. Kolb, M. J. Kurylo, M. J. Molina, A. R. Ravishankara, and S. P. Sander, Chemical kinetics and photochemical data for use in stratospheric modeling, Data evaluation 12, *JPL Publ., 97-4*, 1997.

Dreher, D. B., and R. A. Harley, A fuel-based inventory for heavy-duty diesel truck emissions, *Air Waste Manage. Assoc., 48*, 352-358, 1998.

Eisinger, M., and J. P. Burrows, Tropospheric sulfur dioxide observed by the ERS-2 GOME instrument, *Geophys. Res. Lett., 25,* 4177-4180, 1998.

Eisinger, M., J. P. Burrows, and A. Richter, Studies of the precision of GOME irradiance and radiance products and GOME measurements of OClO and BrO over Antarctica, in *ESA Publication Division (WPP-109), GOME, Global Ozone Monitoring Experiment, Geophysical Validation Campaign*, edited by F. Bednarz, pp. 93-105, Eur. Space Res. and Technol. Cent., Frascati, Italy, 1996.

Emmons, L. K., et al., Climatologies of NO_x and NO_y: A comparison of data and models, *Atmos. Environ.*, *31*, 1851-1904, 1997.

Emmons, L. K., D. A. Hauglustaine, J.-F. Müller, M. A. Carroll, G. P. Brasseur, D. Brunner, J. Staehelin, V. Thouret, and A. Marenco, Data composites of airborne observations of tropospheric ozone and its precursors, *J. Geophys. Res.*, *105*, 20,497-20,538, 2000.

Environmental Protection Agency, *National Air Quality and Emissions Trends Report 1997*, U.S. Environ. Prot. Agency, Off. of Air Quality Plann. and Stand., Res. Triangle Park, N. C., 1998.

Granier, C., J.-F. Müller, S. Madronich, and G. P. Brasseur, Possible causes for the 1990-1993 decrease in the global tropospheric CO abundance; A three-dimensional study, *Atmos. Environ.*, *30*, 1673-1682, 1996.

Granier, C., J.-F. Müller, G. Pétron, and G. Brasseur, A three-dimensional study of the global; CO budget, *Chemosphere Global Change Sci.*, *1*, 255-261, 1999.

Granier, C., J.-F. Müller, and G. Brasseur, The impact of biomass burning on the global budget of ozone and ozone precursors, in *Biomass Burning and its Inter-Relationship with the Climate System*, edited by J. L. Innes, M. Beniston, and M. Verstrate, pp. 69-85, Kluwer Acad., Norwell, Mass., 2000a.

Granier, C., G. Pétron, J.-F. Müller, and G. Brasseur, The impact of natural and anthropogenic hydrocarbons on the tropospheric budget of carbon monoxide, *Atmos. Environ., 34*, 5255-5270, 2000b.

Hao, W. M., and M. H. Liu, Spatial and temporal distribution of tropical biomass burning, *Global Biogeochem. Cycles*, 8, 495-503, 1994.

Hauglustaine, D. A., B. A. Ridley, S. Solomon, P. G. Hess, and S. Madronich, HNO_3/NO_x ratio in the remote troposphere during MLOPEX 2: Evidence for nitrix acid reduction on carbonaceous aerosols?, *Geophys. Res. Lett.*, *23*, 2609-2612, 1996.

Hauglustaine, D. A., G. P. Brasseur, S. Walters, P. J. Rasch, J.-F. Müller, L. K. Emmons, and M. A. Carroll, MOZART: A global chemical transport model for ozone and related chemical tracers, 2, Model results and evaluation, *J. Geophys. Res.*, *103*, 28,291-28,335, 1998.

Hegels, E., D. Perner, P. J. Crutzen, J. P. Burrows, A. Ladstätter-Weißenmayer, M. Eisinger, J. Callies, and W. Balzer, Global Ozone Monitoring Experiment: first BrO measurements, in *XVIII Quadrennial Ozone Sympoisum 1996 L'Aquila Italy Atmospheric Ozone: Proceedings of the Quadrennial Ozone Symposium 1996 Italy 12-21 September 1996*, edited by R. D. Bojkov and G. Visconti, pp. 293-296, Parco Scientifico e Technologico d'Abruzzio, L'Aquila, Italy, 1998.

Holtslag, A., and B. Boville, Local versus nonlocal boundary-layer diffusion in a global climate model, *J. Clim.*, *6*, 1825-1842, 1993.

Hoogen, R., V. V. Rozanov, and J. P. Burrows, Ozone profiles from GOME satellite data: algorithm description and first validation, *J. Geophys. Res., 104*, 8263-8280, 1999.

Horowitz, L. W., and D. J. Jacob, Global impact of fossil fuel combustion on atmospheric NO_x, *J. Geophys. Res.*, *104*, 23,823-23,840, 1999.

Intergovernmental Panel on Climate Change, *Climate Change 1995, The Science of Climate Change*, Cambridge Univ. Press, New York, 1996.

Jähne, B., Signal processing and pattern recognition, in *Handbook of Computer Vision and Applications*, vol. 2, edited by B. Jähne, H. Haussäcker, and P.Geißler, Academic, San Diego, Calif., 1999.

Kato, N., and H. Akimoto, Anthropogenic emissions of SO_2 and NO_x in Asia: Emission inventories, *Atmos. Environ., Part A, 26*, 2997-3017, 1992.

Kiehl, J. T., T. L. Schneider, R. W. Portmann, and S. Solomon, Climate forcing due to tropospheric and stratospheric ozone, *J. Geophys. Res.*, *104*, 31,239-31,254, 1999.

Kraus, A. B., F. Rohrer, E. S. Grobler, and D. Ehhalt, The global tropospheric distribution of NO_x estimated by a three-dimensional chemical tracer model, *J. Geophys. Res.*, *101*, 18,587-18,604, 1996.

Kurosu, T., V. V. Rozanov, and J. P. Burrows, Parameterization schemes for terrestrial water clouds in the radiative transfer model GOMETRAN, *J. Geophys. Res., 102*, 21,809-21,824, 1997.

Lamarque, J.-F., G. P. Brasseur, and P. G. Hess, Three-dimensional study of the relative contributions of the different nitrogen sources in the troposphere, *J. Geophys. Res.*, *101*, 22,955-22,968, 1996.

Lary, D. J., R. Toumi, A. M. Lee, M. Newchurch, M. Pirre, and J. B.

Renard, Carbon aerosols and atmospheric photochemistry, *J. Geophys. Res.*, *102*, 3671-3682, 1997.

Leue, C., Quantitative Analysis of NO_x emissions from GOME satellite image sequences, Ph.D. thesis, Univ. of Heidelberg, Heidelberg, Germany, 1999.

Leue, C., M. Wenig, and U. Platt, Retrieval of tropospheric NO_2 concentration from multispectral image sequences, in *Handbook of Computer Vision and Applications*, vol. 3, chap. 37, edited by B. Jähne, H. Haussäcker, and P. Geißler, pp. 738-805, Academic, San Diego, Calif. 1999.

Leue, C., M. Wenig, T. Wagner, O. Klimm, U. Platt, and B. Jähne, Quantitative analysis of NO_x emissions from GOME satellite image sequences, *J. Geophys. Res.*, *106*, 5493-5505, 2001.

Levy II, H., W. J. Moxim, A. A. Klonecki, and P. S. Kasibhatla, Simulated tropospheric NO_x: Its evaluation, global distribution and individual source contributions, *J. Geophys. Res.*, *104*, 26,279-26,306, 1999.

Logan, J. A., M. J. Parther, S. C. Wofsy, and M. B. McElroy, Tropospheric chemistry: A global perspective, *J. Geophys. Res.*, *86*, 7210-7254, 1981.

Marquard, L. C., T. Wagner, and U. Platt, Improved air mass factor concepts for scattered radiation differential optical absorption spectroscopy of atmospheric species, *J. Geophys. Res.*, *105*, 1315-1327, 2000.

Moxim, W. J., H. Levy II, and P. S. Kasibhatla, Simulated global tropospheric PAN: Its transport and impact on NO_x, *J. Geophys. Res.*, *101*, 12,621-12,638, 1996.

Müller, J.-F., Geographical distribution and seasonal variation of surface emissions and deposition velocities of atmospheric trace gases, *J. Geophys. Res.*, *97*, 3787-3804, 1992.

Müller, J.-F., and G. Brasseur, IMAGES: A three-dimensional chemical transport model of the global troposphere, *J. Geophys. Res.*, *100*, 16,445-16,490, 1995.

Noel, S., M. Buchwitz, H. Bovensmann, R. Hoogen, and J. P.Burrows, Atmospheric water vapour amounts retrieved from GOME satellite data, *Geophys. Res. Lett., 26*, 1841-1844, 1999.

Olivier, J. G. J., A. F. Bouwman, C. W. M. van der Maas, J. J. M. Berdowski, C. Veldt, J. P. J. Bloos, A. J. H. Visschedijk, P. Y. J. Zandveld, and J. L. Haverslag, Description of EDGAR version 2.0: A set of global emission inventories of greenhouse gases and ozone-depleting substances for all anthropogenic and most natural sources on a per country basis and on 1x1 grid, *RIVM Rep. 771060002*, Natl. Inst. of Public Health and the Environ., Bilthoven, Netherlands, 1996.

Parrish, D. D., et al., The total reactive oxidized nitrogen levels and the partitioning between the individual species at six rural sites in eastern North America, *J. Geophys. Res.*, *98*, 2927-2939, 1993.

Penner, J. E., D. J. Bergmann, J. J. Walton, D. Kinnison, M. J. Prather, D. Rotman, C. Price, K. E. Pickering, and S. L. Baughcum, An evaluation of upper tropospheric NO_x with two models, *J. Geophys. Res.*, *103*, 22,097-22,113, 1998.

Pham, M., J.-F. Müller, G. Brasseur, C. Granier, and G. Megie, A three-dimensional study of the tropospheric sulfur cycle, *J. Geophys. Res.*, *100*, 20,061-20,092, 1995.

Platt, U., Differential Optical Absorption Spectroscopy (DOAS), in *Air Monitoring by Spectroscopic Techniques*, chap. 127, edited by M. W. Sigrist, pp. 27-84, John Wiley, New York, 1994.

Price, C., and D. Rind, A simple lightning parameterization for calculating global lightning distributions, *J. Geophys. Res.*, *97*, 9919-9933, 1992.

Richter, A., M. Eisinger, F. Wittrock, and J. P. Burrows, BrO observed from GOME in the Northern Hemisphere in 1997, *Geophys. Res. Lett. 25,* 2683-2686, 1998.

Richter A. and J. P. Burrows, Tropospheric NO_2 from GOME measurements, *Adv. Space Res.*, in press, 2000.

Rozanov, V., D. Diebel, R. J. D. Spurr, and J. P. Burrows, GOMETRAN: A radiative transfer model for the satellite project GOME - the plane parallel version, *J. Geophys. Res., 102*, 16,683-16,695, 1997.

Solomon, S., R. W. Portmann, R. W. Sanders, J. S. Daniel, W. Madsen, B. Bartram, and E. G. Dutton, On the role of nitrogen dioxide in the absorption of solar radiation, *J. Geophys. Res.*, *104*, 12,047-12,058, 1999.

Stamnes, K., S. C. Tsay, W. Wiscombe, and K. Jayaweera, A numerically stable algorithm for discrete-ordinate-method radiative transfer in scattering and emitting layered media, *Appl. Opt.*, *27*, 2502-2509, 1988.

Turman, B. N., and B. C. Edgar, Global lightning distributions at dawn and dusk, *J. Geophys. Res.*, *87*, 1991-1206, 1982.

Valks, P. J. M., and G. J. M. Velders, The present-day and future impact of NO_x emissions from subsonic aircraft on the atmosphere in relation to the impact of NO_x surface sources, *Ann. Geophys.*, *17*, 1064-1079, 1999.

Velders, G. J. M., and C. Granier, Sensitivity of washout on HNO_3/NO_x ratio in atmospheric chemistry models, *J. Geophys. Res., 106*, 3125-3132, 2001.

Vountas, M., V. V. Rozanov, J. P. Burrows, Ring effect: Impact of rotational Raman scattering on radiative transfer in earth's atmosphere, *J. Quant. Spectr. Radiat. Trans., 60*, 943-961, 1998.

Wagner, T., Satellite observations of atmospheric halogen oxides, Ph.D. thesis, Univ. of Heidelberg, Heidelberg, Germany, 1999.

Wagner, T., and U. Platt, Satellite mapping of enhanced BrO concentrations in the troposphere, *Nature, 395*, 486-490, 1998.

Wagner, T., C. Leue, K. Pfeilsticker, and U. Platt, Measurement of atmospheric BrO and OClO by GOME, in *Proceedings of the European Symposium on Atmospheric Measurements from Space (ESAMS 99),* 18-22 January 1999, pp. 415-419, Eur. Space Res. and Technol. Cent., Noordwijk, Netherlands, 1999.

Wang, Y., J. A. Logan, and D. J. Jacob, Global simulation of tropospheric O_3-NO_x-hydrocarbon chemistry, 2, Model evaluation and global ozone budget, *J. Geophys. Res.*, *103*, 10,727-10,755, 1998.

Wenig, M., C. Leue, B. Jähne, and U. Platt, Cloud classification using image sequences of GOME data, in *Proceedings of the European Symposium on Atmospheric Measurements from Space (ESAMS 99),* 18-22 January 1999, pp. 420-424, Eur. Space Res. and Technol. Cent., Noordwijk, Netherlands, 1999.

World Meteorological Organization, Scientific assessment of ozone depletion: 1998, edited by D. Albritton et al., *Rep. 44*, Global Ozone Res. and Monit. Proj., Geneva, 1999.

J. P. Burrows and A. Richter, Institute of Environmental Physics, University of Bremen, P.O. Box 330440, 28334 Bremen, Germany.

C. Granier, Aeronomy Laboratory, NOAA, 325 Broadway, Boulder, CO 80303.

K. Pfeilsticker, U. Platt, T. Wagner, and M. Wenig, Institut für Umweltphysik, University of Heidelberg, Im Neuenheimer Feld 229, 69120 Heidelberg, Germany.

R. W. Portmann, Aeronomy Laboratory, NOAA, 325 Broadway, Boulder, CO 80303.

G. J. M. Velders, Air Research Laboratory, National Institute of Public Health and the Environment (RIVM), P.O. Box 1, 3720 BA Bilthoven, Netherlands. (guus.velders@rivm.nl)

(Received May 22, 2000; revised October 19, 2000;
accepted November 21, 2000.)